Article

Current Biology

Capping Protein Insulates Arp2/3-Assembled Actin Patches from Formins

Graphical Abstract

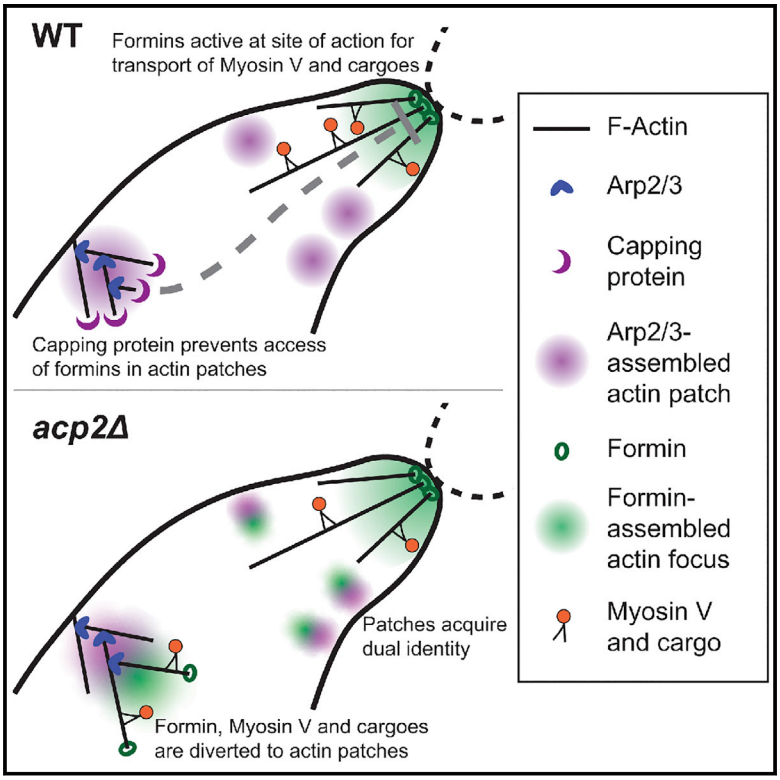

Highlights

- Capping proteins prevent access of formins to Arp2/3-nucleated actin patches
- Formins at uncapped Arp2/3 patches form actin structures of mixed identity
- Formin activity at these ectopic sites leads to diversion of myosins and cargoes
- Capping protein β subunit shows specific competition with the formin knob region

Authors

Ingrid Billault-Chaumartin, Sophie G. Martin

Correspondence

sophie.martin@unil.ch

In Brief

How do cells maintain functionally distinct actin structures in a common cytosol? Billault-Chaumartin and Martin show that competition between capping proteins and formins keeps formins off Arp2/3-assembled structures. Formin activity at uncapped Arp2/3 patches forms mixed-identity actin structures, which divert myosins from their site of action.

Billault-Chaumartin & Martin, 2019, Current Biology 29, 3165–3176
October 7, 2019
https://doi.org/10.1016/j.cub.2019.07.088

CellPress

Current Biology
Article

CellPress

Capping Protein Insulates Arp2/3-Assembled Actin Patches from Formins

Ingrid Billault-Chaumartin[1] and Sophie G. Martin[1,2,*]
[1]Department of Fundamental Microbiology, Faculty of Biology and Medicine, University of Lausanne, 1015 Lausanne, Switzerland
[2]Lead Contact
*Correspondence: sophie.martin@unil.ch
https://doi.org/10.1016/j.cub.2019.07.088

SUMMARY

How actin structures of distinct identities and functions coexist within the same environment is a critical self-organization question. Fission yeast cells have a simple actin cytoskeleton made of four structures: Arp2/3 assembles actin patches around endocytic pits, and the formins For3, Cdc12, and Fus1 assemble actin cables, the cytokinetic ring during division, and the fusion focus during sexual reproduction, respectively. The focus concentrates the delivery of hydrolases by myosin V to digest the cell wall for cell fusion. We discovered that cells lacking capping protein (CP), a heterodimer that blocks barbed-end dynamics and associates with actin patches, exhibit a delay in fusion. Consistent with CP-formin competition for barbed-end binding, Fus1, F-actin, and the linear filament marker tropomyosin hyper-accumulate at the fusion focus in cells lacking CP. CP deletion also rescues the fusion defect of a mutation in the Fus1 knob region. However, myosin V and exocytic cargoes are reduced at the fusion focus and diverted to ectopic foci, which underlies the fusion defect. Remarkably, the ectopic foci coincide with Arp2/3-assembled actin patches, which now contain low levels of Fus1. We further show that CP localization to actin patches is required to prevent the formation of ectopic foci and promote efficient cell fusion. During mitotic growth, actin patches lacking CP similarly display a dual identity, as they accumulate the formins For3 and Cdc12, normally absent from patches, and are co-decorated by the linear filament-binding protein tropomyosin and the patch marker fimbrin. Thus, CP serves to protect Arp2/3-nucleated structures from formin activity.

INTRODUCTION

Cells simultaneously contain several actin-based structures that need to be tailored to their specific function, with a specific architecture, size, lifetime, and set of actin-binding proteins. The architecture is defined in part by the nucleator [1, 2]: Arp2/3 promotes the assembly of branched structures, whereas other nucleators, in particular formins, assemble linear ones. Arp2/3-assembled dendritic networks generate pushing forces against membranes, for instance in the lamellipodium of migrating cells, to drive the movement of intracellular bacteria, or to promote internalization of endocytic vesicles in yeast actin patches. Formin-nucleated actin structures consist of linear filaments, which can be bundled for protrusive or contractile force generation, for instance in filopodia or cytokinetic contractile rings, or which underlie long-range myosin-based transport.

The principles underlying the assembly of distinct actin structures at the same time are beginning to be understood. First, competition is an important factor. For instance, diverse filamentous actin (F-actin) structures are in competition for a limited pool of actin monomers [3]. This competition is modulated by profilin, which favors F-actin assembly by formins and other nucleators over Arp2/3 [4, 5]. Second, specific actin nucleators confer part of the structure's identity: formins promote the formation of more flexible filaments [6], favoring tropomyosin association [7]; different formins may even promote association of distinct tropomyosin isoforms [8]. Third, self-assembly principles govern the segregation of specific actin-binding proteins to diverse structures. For instance, cooperative loading and competition between fimbrin and tropomyosin drive their association to distinct actin structures [9]. Therefore, *in vivo*, tropomyosin preferentially associates with formin-assembled structures and fimbrin with Arp2/3-nucleated actin patches [10, 11].

Capping protein (CP) is present in cells in micromolar concentration, similar to the concentration of actin filament barbed ends, and binds the barbed end to arrest dynamics [12]. CP forms a heterodimer of structurally similar α and β subunits, both of which harbor a mobile C-terminal extension, called the tentacle, which contributes to barbed-end binding [13–15]. CP lacking both tentacles forms a stable complex but does not bind actin, with the α tentacle playing a more critical role than the β tentacle [14, 16]. CP activity is further regulated by binding partners bearing a CP interaction (CPI) motif [17]: CP-carrying mutations blocking CPI binding retain capping activity *in vitro* but lose localization and function *in vivo*, indicating that binding partners are required for activity *in vivo* [18]. The Aim21-Tda2 complex, which binds CP through the same residues, modulates CP recruitment and activity at actin patches in *S. cerevisiae* [19, 20]. By keeping filaments short, CP plays a major role in the force production of dendritic networks [21]. Indeed, absence of CP leads to loss of the lamellipodium in migrating cells [22, 23] and excess actin filaments in yeast actin patches, which exhibit a longer lifetime [16, 24–26].

As formins and CP both interact with actin filament barbed ends but promote opposite activities—i.e., extension versus

capping—they compete with each other *in vitro* [27–30]. Recent single-molecule work showed formin and CP simultaneously binding the filament barbed end, forming a ternary "decision complex" intermediate [31, 32]. Evidence for competition *in vivo* was shown in the fission yeast *Schizosaccharomyces pombe*, where CP deletion ameliorates the cell-division phenotype of a hypomorphic formin *cdc12* allele [33]. CP may also compete with formins in filopodia [34]. In addition, CP is well established to compete with ENA/VASP both *in vitro* and *in vivo*, where this competition controls filopodium formation [12, 35]. Whether such competition contributes to actin structure identity has not been explored.

The fission yeast represents a simple system to dissect the mechanisms governing actin structure identities. This cell contains only four actin structures, actin patches, cables, ring, and focus, each of which fulfils a specific function [1, 36]. Arp2/3 nucleates actin patches, marked by fimbrin Fim1, around invaginating endocytic vesicles, which assemble in a stereotypical manner [37, 38] and provide force for vesicle internalization [39]. CP localizes to actin patches [33, 40, 41], where it limits actin incorporation and helps force production [16, 24–26]. Interestingly, although active CP is a heterodimer, deletion of the α and β subunits (Acp1 and Acp2, respectively) does not produce exactly the same phenotype [24]. Three formins nucleate distinct linear F-actin structures: Cdc12 assembles the contractile actin ring; For3 assembles linear actin cables that underlie long-range myosin-based transport for polarized cell growth; and Fus1 is expressed specifically during mating and nucleates the fusion focus, an F-actin aster that concentrates secretory vesicles transported by myosin V Myo52 [42, 43]. These vesicles carry cell-wall hydrolases, which digest the cell wall for cell fusion. The coalescence of the fusion focus also requires tropomyosin Cdc8 [44], and a visual screen revealed Cdc8 functions together with the type V myosin Myo51 [45]. This same screen identified fusion defects in cells lacking *acp2*.

Starting from the hypothesis that CP and formin Fus1 compete during fusion focus assembly, we discovered that CP protects actin patches against formin activity. In the absence of CP, Fus1 binds barbed ends in actin patches, forming ectopic foci that divert secretory vesicles away from the site of cell-cell contact and compromise fusion. Similarly, in proliferating cells lacking CP, the formins For3 and Cdc12 are ectopically recruited to actin patches, which exhibit a dual identity manifested by co-decoration with fimbrin and tropomyosin. Thus, CP ensures actin structure identity by insulating Arp2/3-assembled structures against formins.

RESULTS

Capping Protein Is Required for Efficient Cell-Cell Fusion

To investigate the role of CP in cell fusion, we first assessed the fusion efficiency of strains lacking one or both CP subunits (*acp1Δ*, *acp2Δ*, *acp1Δ acp2Δ*). After 12 h of starvation, these strains exhibited a reduced fraction of fused zygotes compared to wild type (WT), which increased 36 h post starvation (Figure 1A), indicating that CP deletion causes a fusion delay. The duration of the fusion process, from initial formation of the Myo52-labeled fusion focus in both partner cells [42] to cytoplasmic mixing, defined by entry in the M cell of cytosolic GFP expressed in P cells, was significantly longer in CP-lacking cells (Figures 1B and 1C). The fusion focus also persisted significantly longer post fusion in CP-lacking cells (Figures 1D and 1E). Both phenotypes were clear in all mutant combinations but strongest in *acp2Δ* single mutant, on which we focused most of our attention. Thus, CP promotes fusion, because its absence causes fusion delay and persistence of the fusion focus after fusion.

Formin Fus1 and F-Actin Excessively Accumulate at the Fusion Site in the Absence of Capping Protein

Consistent with CP preventing filament barbed-end extension, previous work reported that Arp2/3-assembled actin patches lacking CP accumulate more actin [24, 41]. To investigate the organization of F-actin during fusion, we first used GFP-CHD as F-actin marker [46, 47]. Like in interphase cells, actin patches appeared brighter in *acp2Δ* than WT cells during mating (Figure 2A) [24]. *acp2Δ*, *acp1*Δ, and *acp1*Δ *acp2*Δ cells also displayed slightly more F-actin at the position of the fusion focus (Figures 2A, 2D, and S1A). Because GFP-CHD measurements at the fusion site cannot distinguish between F-actin in the fusion focus or in surrounding patches, we probed the localization of specific fusion focus components. Fus1 accumulated approximately 4-fold more in *acp2*Δ, *acp1*Δ, and *acp1*Δ *acp2*Δ cells than in WT cells at the fusion focus (Figures 2B, 2D, and S1B). Global Fus1-sfGFP fluorescence levels also increased 1.6-fold (Figure S1D). Tropomyosin Cdc8, which preferentially binds formin-assembled filaments [7, 44, 48–50], increased about 2-fold at the fusion focus of *acp2*Δ compared to WT cells (Figures 2C, 2D, and S1C). Thus, the absence of CP leads to increased F-actin and associated proteins at the fusion focus.

The dramatic Fus1 increase in *acp2Δ* fusion foci is consistent with the proposed competition between formins and CP for barbed-end binding [31–33]. We note that CP levels were mildly increased in *fus1*Δ (1.1-fold; Figures S2A and S2B). To probe the hypothesis that CP promotes cell fusion by limiting Fus1-driven actin polymerization at the fusion focus, we tested whether (1) Fus1 overexpression mimics loss of CP, (2) reducing Fus1 activity ameliorates fusion efficiency in the absence of CP, and (3) CP localizes to the fusion focus. First, Fus1 overexpression had no effect on fusion duration, fusion focus persistence, or ectopic Myo52 foci (Figures S2C–S2E; see below regarding ectopic foci). However, the overexpression increased total Fus1 but not Fus1 at the fusion focus (Figure S2D). Thus, Fus1 overexpression does not directly mimic loss of CP. Second, we constructed four Fus1 alleles mutated in the FH2 domain. Although all mutants abolished actin assembly *in vitro* [51], they showed different phenotypes when introduced as sole copy at the native genomic locus of otherwise WT cells. Fus1^{K879A} and Fus1^{K1112A}, which carry mutations in the FH2 lasso, were partly fusion competent, whereas Fus1^{I951A} and Fus1^{G1087R,N1088P}, which carry mutations in the FH2 knob and post, respectively, almost completely blocked cell fusion. Combining these *fus1* alleles with the *acp2*Δ phenotype did not systematically ameliorate the fusion phenotype (Figures 2E and 2F). In particular, the two hypomorphic lasso mutants compromised fusion further in *acp2*Δ. By contrast, the fusion-incompetent *fus1^{I951A}* allele permitted high levels of fusion in *acp2Δ*. This reveals an allele-specific suppression, where the Fus1 knob but not lasso

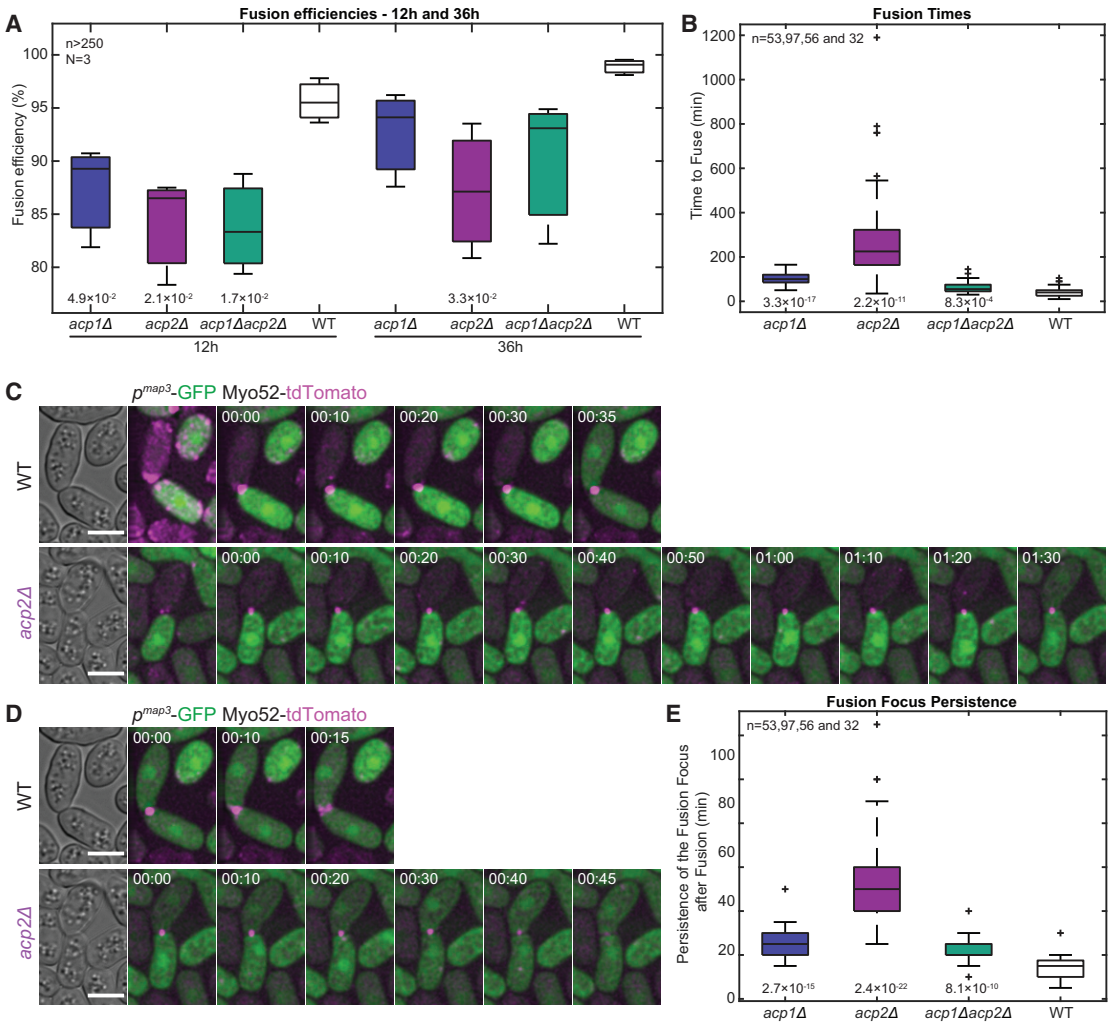

Figure 1. CP Deletion Leads to Fusion Delay and Fusion Focus Persistence after Fusion

(A) Fusion efficiencies 12 and 36 h after nitrogen removal in the indicated strains.

(B) Fusion times in the indicated strains.

(C) Time-lapse images of Myo52-tdTomato and cytosolic GFP expressed in P cells under the *map3* promoter in WT and *acp2*Δ, from the beginning to end of the fusion process. The times shown (in h:min) are relative to the initial formation of the fusion focus.

(D) Time-lapse images of strains as in (C) from the time of fusion taking place up to the disappearance of the fusion focus. The times shown (in h:min) are relative to the time of fusion. Note that the first image (at 00:00) is the same as the last image in (C).

(E) Fusion focus persistence times in the indicated strains.

All indicated p values are relative to WT. Scale bars represent 5 μm.

mutants compromise competition with CP. This finding is consistent with the recently proposed steric clash between the FH2 knob and the CP β tentacle [31]. Third, Acp1 and Acp2 tagged with sfGFP localized prominently to actin patches, but neither was detected at the fusion focus in either WT cells or cells lacking the other CP subunit (Figures 5A, 5C, 5D, and 5F). Thus, CPs are largely absent from the fusion focus, suggesting that competition with Fus1 principally takes place elsewhere.

Absence of Capping Protein Leads to Reduced Levels of Myosin V and Cargoes at the Fusion Focus and Formation of Ectopic Foci

Despite higher Fus1 levels, myosin Myo52 was reduced about 2-fold at the fusion focus in *acp2*Δ compared to WT cells (Figures 1C and 3F). A similar reduction was observed in *acp1Δ* and *acp1Δ acp2Δ* cells (Figure S3A). Similarly, exocytic vesicles marked by the exocyst subunits Exo84 and Exo70, the Rab11 homolog Ypt3, and the glucanase cargoes Agn2 and Eng2 were all reduced at the focus at fusion time in CP-lacking strains (Figures 3A–3F and S3B–S3F). Because these glucanases are responsible for degrading the cell wall for fusion [42], their reduced accumulation at the focus is the likely cause of the *acp2*Δ fusion delay.

Why do the actin-rich *acp2Δ* fusion foci accumulate fewer exocytic vesicles? We noticed that *acp2*Δ cells frequently form Myo52 foci away from the fusion focus (Figure 3G). Such ectopic foci formed in both P and M cells repeatedly during the fusion process. In time-lapse imaging at 5-min intervals, *acp2*Δ cells

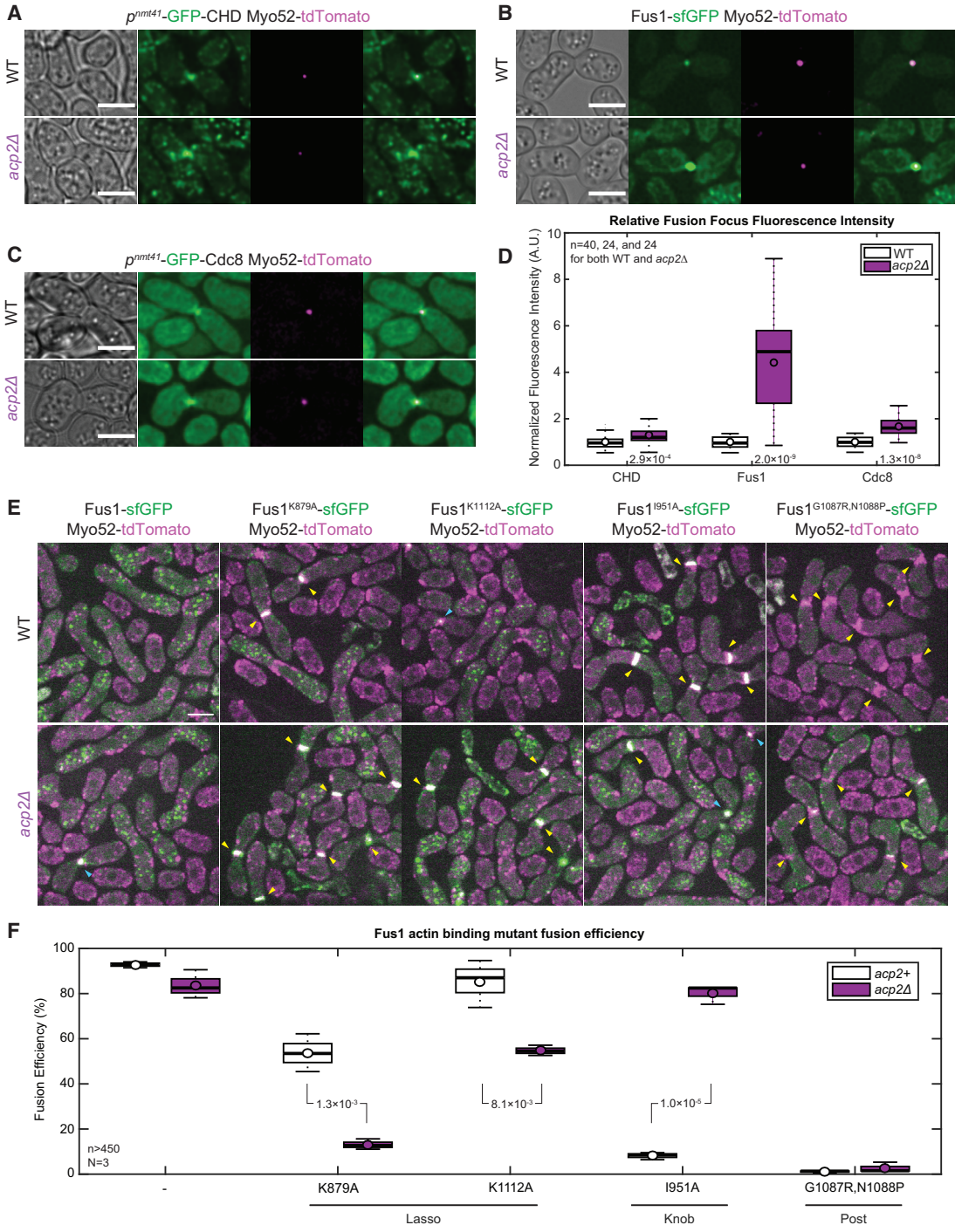

Figure 2. CP Deletion Leads to Increased Actin, Tropomyosin, and Fus1 at the Fusion Focus

(A–C) Myo52-tdTomato and (A) GFP-CHD labeling F-actin, (B) Fus1-sfGFP, and (C) GFP-Cdc8 in WT and *acp2*Δ at fusion time.

(D) Fusion focus fluorescence intensities normalized to WT at fusion time in strains as in (A)–(C). See Figures S1A–S1C for full fluorescence profile measurements.

(E) Spinning-disk confocal images of Myo52-tdTomato and WT or mutant Fus1-sfGFP, as indicated, in WT and *acp2*Δ. Yellow arrowheads point to unfused cell pairs, with a broad Fus1 and Myo52 distribution at the contact zone. Blue arrowheads point to fusion foci.

(F) Fusion efficiencies at 9 h after nitrogen removal in WT or *acp2*Δ strains carrying WT or mutant *fus1*, as indicated.

All p values are relative to WT, except where indicated. Scale bars represent 5 μm. See also Figures S1 and S2.

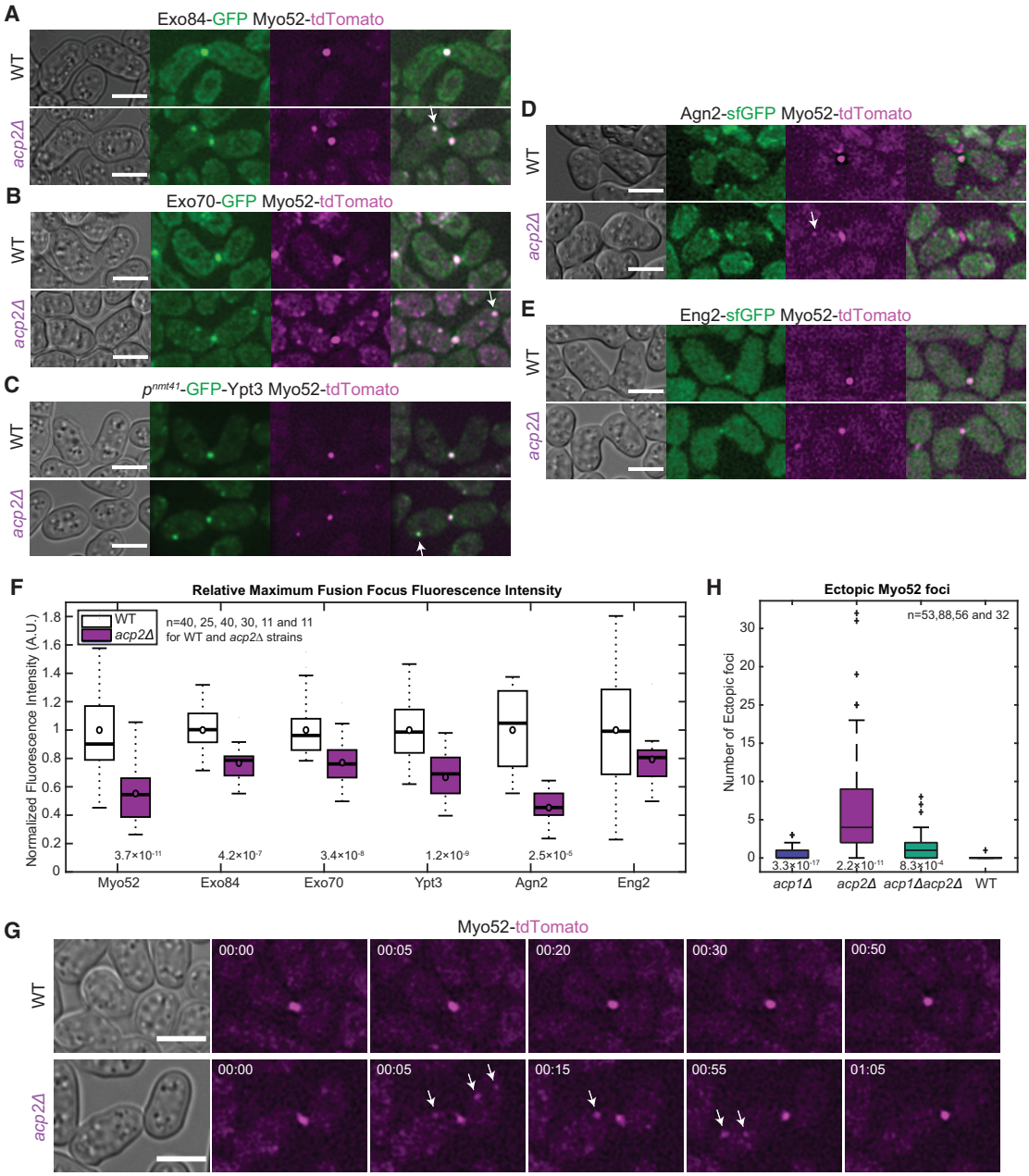

Figure 3. CP Deletion Leads to Reduced Vesicular Markers at the Fusion Focus and Formation of Ectopic Foci

(A–E) Myo52-tdTomato and (A) Exo84-GFP, (B) Exo70-GFP, (C) GFP-Ypt3, (D) Agn2-sfGFP, and (E) Eng2-sfGFP in WT and *acp2*Δ before fusion time. White arrows highlight ectopic foci. Note that these images, selected to show ectopic foci, stem from various time points during time-lapse imaging, for which specific timing in the fusion process and photobleaching may mask the difference in fusion focus intensity.

(F) Fusion focus fluorescence intensities at fusion time normalized to WT in the strains mentioned in (A)–(E).

(G) Time-lapse images of Myo52-tdTomato in WT and *acp2Δ* during the fusion process. White arrows show ectopic Myo52 foci. Time is in h:min.

(H) Number of time frames at which a Myo52 ectopic focus was observed during the fusion process in time-lapse imaging as in (G).

All p values are relative to WT. Scale bars represent 5 μm. See also Figure S3 and Video S1.

displayed on average 7 time points with ectopic foci, *acp1*Δ and *acp1*Δ *acp2*Δ cells displayed 1, and we barely found any for WT cells with this set-up (a single ectopic focus in 32 mating pairs; Figure 3H). Camera upgrade (which happened in the course of the project) and spinning-disk imaging revealed more ectopic foci in all backgrounds, including WT (see Figures 5J and 4A, respectively). The rare, transient ectopic foci detected in WT mating pairs (see Figure 1C, 10-min time frames, for example) suggest that the *acp2*Δ behavior exists but is normally repressed in WT cells. These ectopic foci extensively colocalized with Exo84, Exo70, and Ypt3 (Figures 3A–3C and S3G–S3I). We could not detect glucanases at ectopic foci, likely because of low

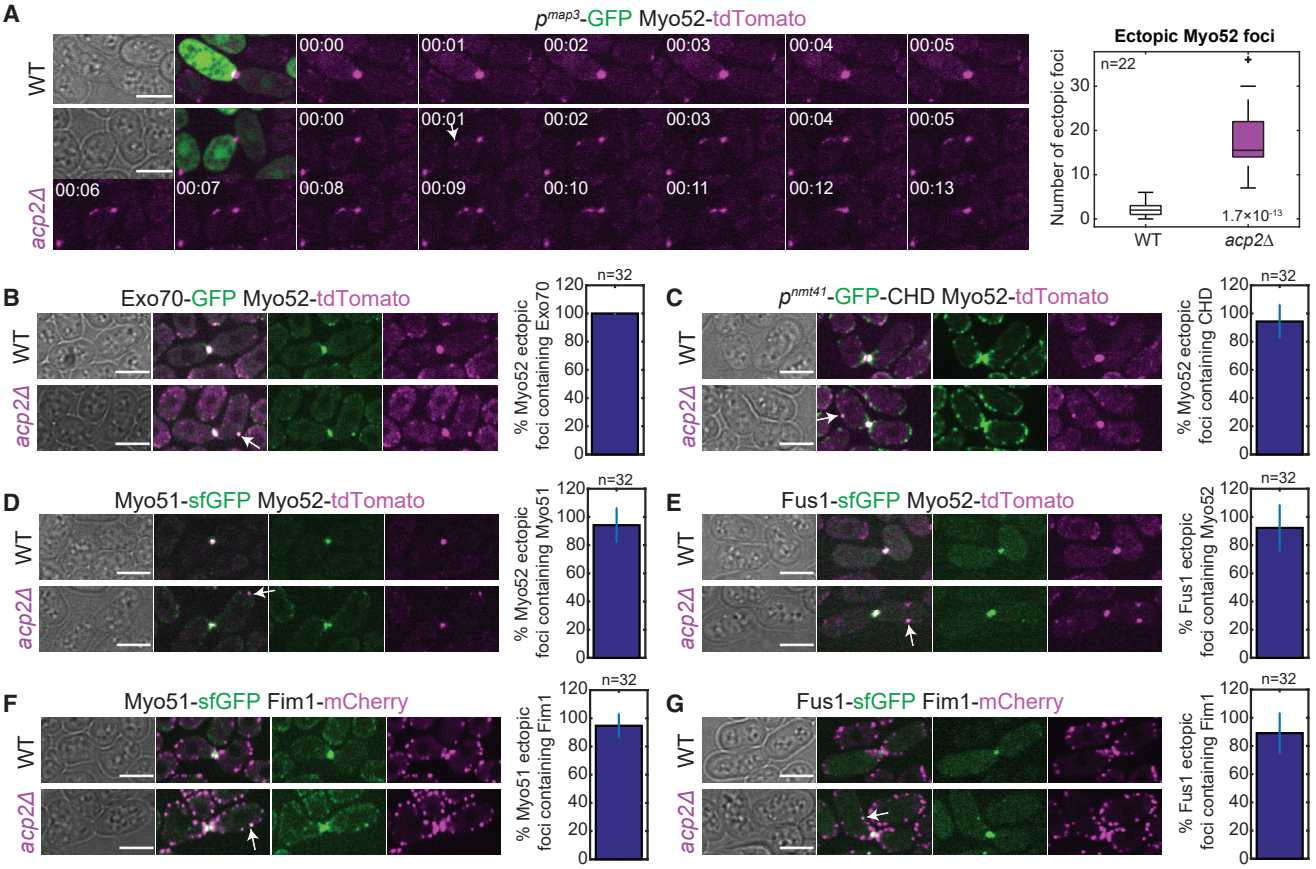

Figure 4. Myo52 Ectopic Foci Form at Actin Patches

(A) Spinning-disk confocal time-lapse images of Myo52-tdTomato and cytosolic GFP expressed under the *map3* promoter (shown only for the first time point) in WT and *acp2*Δ before fusion time. The white arrow marks an ectopic Myo52 focus that forms at 1 s and then moves toward the fusion focus. Time is in min:s. Right: number of time points, acquired at 1-s intervals during 3 min, displaying a Myo52 ectopic focus.

(B–E) Spinning-disk confocal images of Myo52-tdTomato and (B) Exo70-GFP, (C) GFP-CHD, (D) Myo51-sfGFP, and (E) Fus1-sfGFP in WT and *acp2*Δ before fusion time.

(F and G) Spinning-disk confocal images of strains expressing Fim1-mCherry and (F) Myo51-sfGFP or (G) Fus1-sfGFP in WT and *acp2*Δ before fusion time.

The bar plots to the right of the images show the proportion of ectopic foci colocalizing with the indicated markers, of which an example is shown with a white arrow. Scale bars represent 5 μm. See also Figure S4 and Videos S2, S3, and S4.

expression levels and reduction of function by sfGFP tagging (Figures 3D and 3E). These results suggest that the formation of ectopic foci is the cause of the reduced Myo52 and cargoes at the fusion focus.

Myo52 Ectopic Foci Form at Actin Patches

Higher-speed time-lapse spinning-disk imaging at 1-s intervals showed Myo52 ectopic foci did not appear randomly: they did not break off from the fusion focus; instead, they formed and stayed at remote locations at the cell periphery, occasionally moving back and fusing with the fusion focus (Figure 4A; Video S1). The colocalization with exocytic markers stood true at this higher temporal resolution (Figure 4B). Thus, ectopic foci are nucleated at a remote location in the absence of CP.

Interestingly, GFP-CHD as F-actin marker revealed that >90% of ectopic foci colocalized, at least transiently, with what looked like actin patches (Figure 4C). Ectopic foci also colocalized with Myo51, a second type V myosin that normally associates with tropomyosin and decorates linear actin structures [45, 52, 53] (Figure 4D). Whereas Myo51 principally decorates the fusion focus in WT cells, in *acp2Δ* it additionally localized to actin patches marked by the actin bundler Fim1 [54, 55] (Figure 4F). Importantly, the more sensitive spinning-disk microscopy also revealed Fus1 in Myo52 ectopic foci (Figure 4E; Video S2), which colocalized with Fim1 (Figure 4G; Video S3). Fus1 also colocalized with Myo52 ectopic foci in *acp1Δ acp2Δ* double mutants (Figure S4; Video S4). Thus, the absence of CP leads to recruitment of formin Fus1 and type V myosin to Arp2/3-nucleated actin patches.

Fus1 likely binds exposed filament barbed ends at actin patches in the absence of CP, and nucleates ectopic foci. To investigate whether CP's capping function is required to protect patches from Fus1, we deleted Acp1 and Acp2 tentacles (*acp1*$^{\Delta t}$ and *acp2*$^{\Delta t}$) to reduce CP affinity for actin barbed ends. These truncations compromised actin patch localization, with Acp2$^{\Delta t}$ retaining better localization than Acp1$^{\Delta t}$ (Figures 5B, 5E, and 5H), in agreement with previous *in vitro* work [14]. They also showed more frequent ectopic Myo52 foci than WT cells, in an

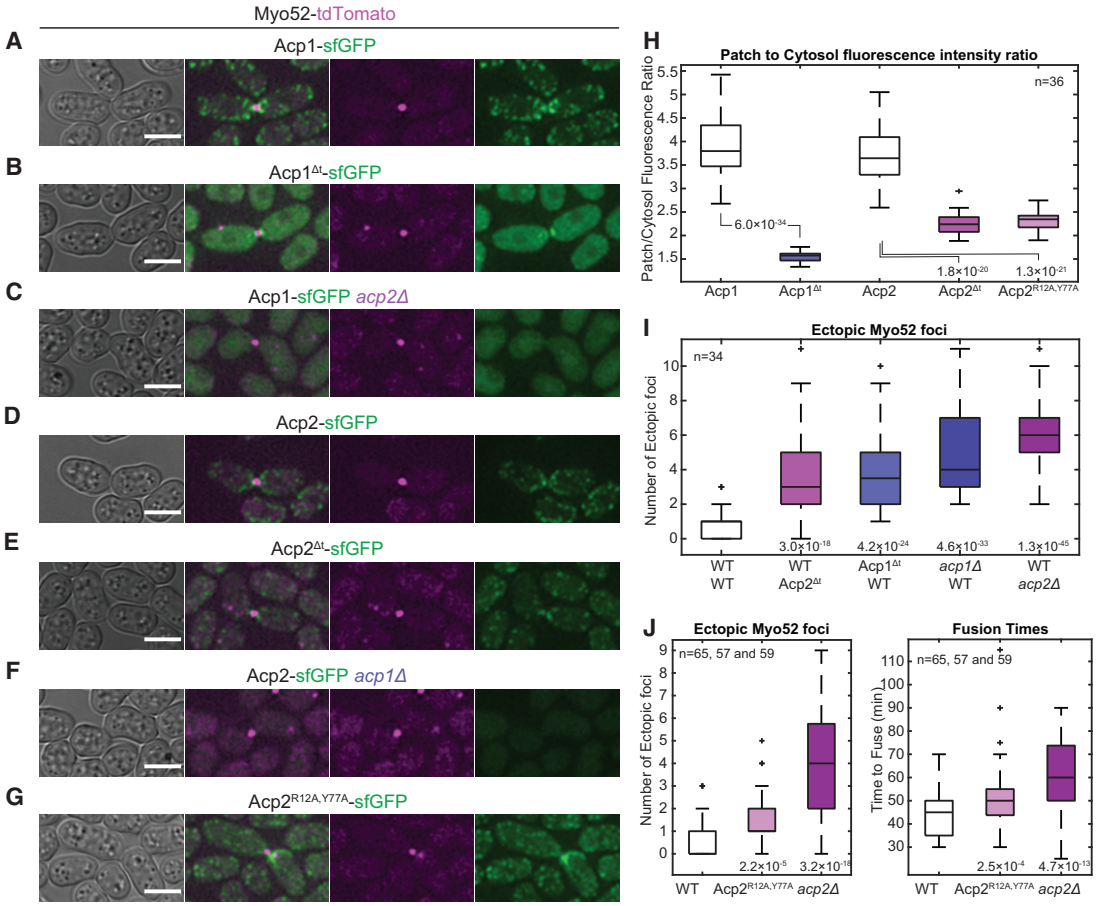

Figure 5. CP Recruitment to Actin Patches and Barbed-End Binding Is Required to Protect against Ectopic Foci

(A–G) Myo52-tdTomato- (A) Acp1-sfGFP, (B) Acp1$^{\Delta t}$-sfGFP, (C) Acp1-sfGFP in *acp2Δ*, (D) Acp2-sfGFP, (E) Acp2$^{\Delta t}$-sfGFP, (F) Acp2-sfGFP in *acp1Δ*, or (G) Acp2^{R12A,Y77A}, carrying mutated CPI-interacting residues, at fusion time, as indicated. Scale bars represent 5 μm.

(H) Acp1-sfGFP and Acp2-sfGFP patch-to-cytosol fluorescence intensity ratios in fusing cells of strains as in (A)–(G).

(I) Number of time frames at which a Myo52 ectopic focus was observed during the fusion process in time-lapse imaging of strains as in (A)–(F).

(J) Ectopic foci (as in I) and fusion times for WT (*acp2-sfGFP*), *acp2*^{R12A,Y77A}*-sfGFP*, and *acp2*Δ strains.

All p values are relative to WT. See also Figure S5.

order consistent with their retained actin-binding capacity (Figures 5B, 5E, and 5I). We also generated *acp2*^{R12A,Y77A}, predicted not to bind the CPI motif [18]. Acp2^{R12A,Y77A} localized inefficiently to patches (Figures 5G and 5H), and exhibited ectopic foci and increased fusion times, to levels intermediate between WT and *acp2*Δ cells (Figure 5J). The reduced localization of Acp1$^{\Delta t}$, Acp2$^{\Delta t}$, and Acp2^{R12A,Y77A} to actin patches was not due to reduced F-actin content in the patches, which instead exhibited increased LifeAct-mCherry fluorescence (Figures S5A and S5B), like *acp2Δ* cells [24]. These results indicate that localization of CP to patches is necessary to prevent the formation of ectopic foci.

Finally, to test whether ectopic foci cause the fusion delay by diverting vesicles away from the cell-cell contact zone, we artificially recruited Myo52-GFP to patches labeled with Fim1-GBP-mCherry by using the high affinity between GFP-binding protein (GBP) and GFP (Figures S5C–S5E). This led to fusion delay and focus persistence after fusion, replicating the *acp2*Δ phenotypes (Figures 1B, 1E, and S5C–S5E).

We conclude that during fusion, CP insulates actin patches from Fus1. This ensures Fus1 activity is restricted, and myosin V-driven cargoes are directed, to the site of cell-cell contact.

Uncapped Actin Patches Recruit Formins and Acquire a Dual Identity in Interphase Cells

To test whether CP more generally protects actin patch identity, we investigated the influence of CP deletion in interphase cells. In the absence of CP, actin patches are dispersed both in *S. cerevisiae* [56] and in *S. pombe* [24, 41], and *S. pombe* cells also exhibit weak actin cables [33, 41]. Remarkably, markers normally associated with formin-nucleated actin cables were perturbed in *acp2Δ*: Myo51, which labels cable-like structures in WT cells [53], formed punctate structures that colocalized with Fim1 in *acp2*Δ cells (Figure 6A); Myo52, which mainly localizes to cell tips in WT cells, formed dots that coincided with Myo51 and Fim1 patches in *acp2*Δ (Figures 6B and 6C); and tropomyosin Cdc8, which stabilizes actin cables and is largely absent from actin patches in WT cells, formed foci that

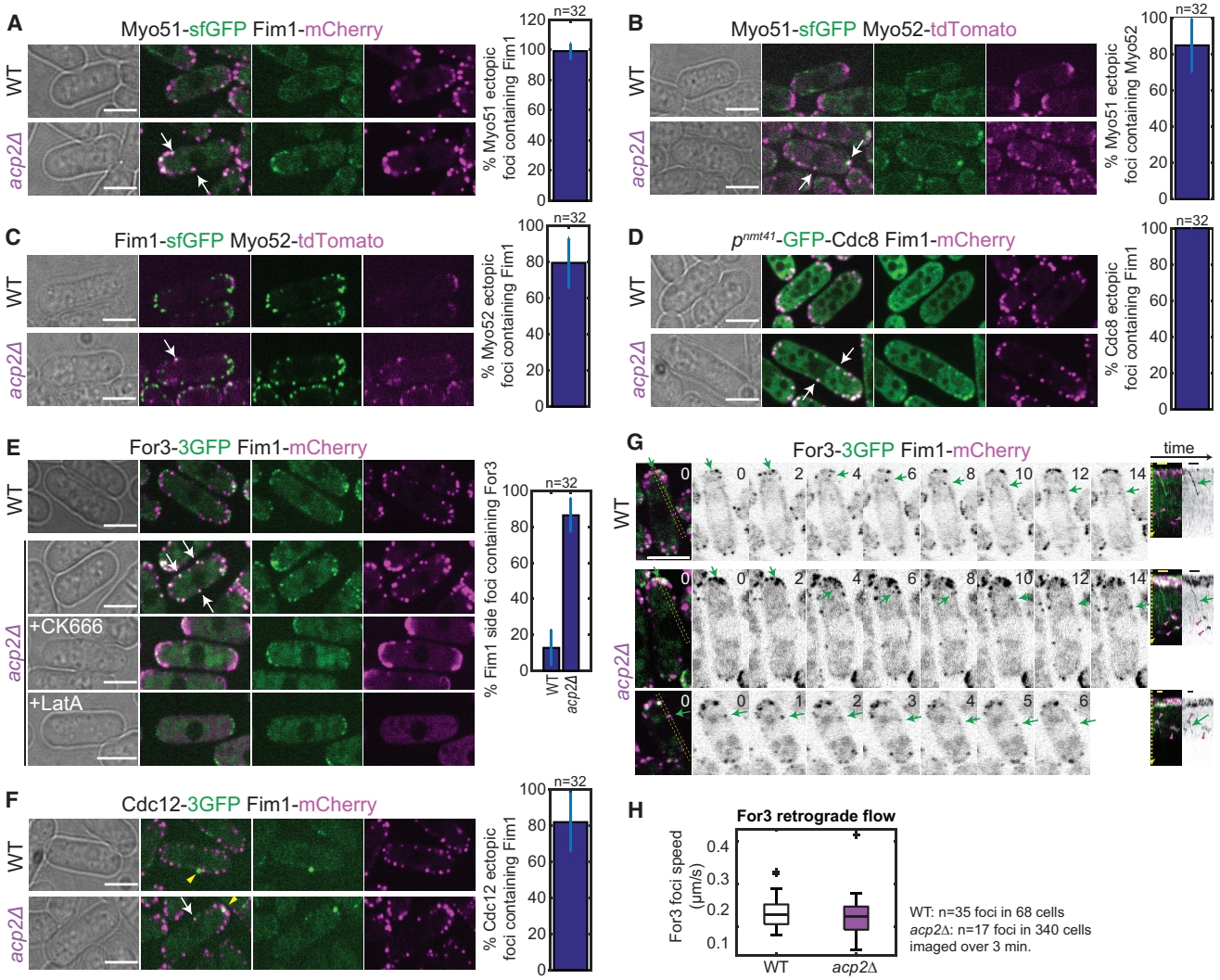

Figure 6. CPs Insulate Actin Patches from Myo52 and Actin Cable Markers in Interphase Cells

(A–F) Spinning-disk confocal images of (A) Fim1-mCherry and Myo51-sfGFP, (B) Myo52-tdTomato and Myo51-sfGFP, (C) Myo52-tdTomato and Fim1-sfGFP, (D) Fim1-mCherry and GFP-Cdc8, (E) Fim1-mCherry and For3-3GFP, and (F) Fim1-mCherry and Cdc12-3GFP in WT and *acp2Δ* interphase cells. In (E), bottom panels show *acp2Δ* treated with 500 μM CK-666 for 5 min or 200 μM latrunculin A for 5 min. White arrows highlight colocalization events in *acp2Δ*, which do not occur in WT cells. Yellow arrowheads point to Cdc12 spots. The proportion of colocalization at ectopic sites along the cell sides is shown with the bar plot on the right.

(G) Spinning-disk confocal time-lapse images of Fim1-mCherry and For3-3GFP (green and gray) showing retrograde flow in WT (top) and *acp2Δ* cells (bottom two panels). Bottom: an example of retrograde flow starting at a lateral actin patch. Kymographs of the yellow dashed boxed regions are shown on the right. Green arrows point to For3-3GFP retrograde flow. Purple arrowheads in kymographs show lateral actin patches on which For3 localizes in *acp2Δ* but not WT cells.

(H) For3 retrograde flow rate.

Time is in s. Scale bars represent 5 μm. See also Figure S6 and Videos S5 and S6.

colocalized with Fim1 in *acp2*Δ (Figure 6D; Video S5). The coincidence of fimbrin and tropomyosin is particularly remarkable given recent data showing that competition between these two proteins drives their sorting to distinct Arp2/3- and formin-nucleated networks, respectively [9]. Thus, actin patches assume a dual identity in the absence of CP both during mating and during vegetative growth.

Because Fus1 is not expressed during mitotic growth [43], we monitored the localization of For3 and Cdc12 formins. For3, which only occasionally overlapped with actin patches in WT cells, was prominently present at actin patches in *acp2Δ* mutants (Figure 6E; Video S6). By contrast, in *fim1Δ* cells, in which tropomyosin also decorates patches [11], For3 was largely absent from patches like in WT cells (Figure S6A). In *acp2Δ* cells, disruption of patches with the Arp2/3 inhibitor CK-666 or F-actin depolymerization with latrunculin A restored For3 localization to cell poles (Figure 6E). Arp2/3 inhibition also promoted Fim1 relocalization to cell poles, which is likely due to excess formin-assembled cables [3], as complete actin depolymerization rendered Fim1 cytosolic (Figure 6E). Thus, uncapped actin patches ectopically recruit For3. Cdc12 also formed ectopic foci at actin patches in *acp2Δ* cells (Figure 6F). These ectopic

foci were distinct from the previously reported spot of Cdc12 [57], which also occurs in WT cells, does not coincide with patches, has a longer lifetime, and is more intense (Figure 6F). We conclude that formins are recruited to uncapped actin patches.

To address whether formins are active at patches, we first tested whether their inactivation would alleviate the localization of tropomyosin at *acp2Δ* actin patches. However, deletion of *for3* by itself led to significant Cdc8 enrichment on actin patches, likely because actin cytoskeleton homeostasis is perturbed in the absence of actin cables (Figure S6B). Therefore, not surprisingly, Cdc8 also localized to actin patches in *for3Δ acp2Δ* and *cdc12-112 for3Δ acp2Δ* mutants (Figures S6B and S6C). We then directly probed for For3 activity by observing its retrograde flow, which depends on actin assembly in cables [47]. For3 retrograde flow occurred at similar rates in WT and *acp2Δ* cells, although fewer movements were observed in *acp2Δ*, consistent with the weak actin cables (Figures 6G and 6H) [33, 41]. Interestingly, For3 linear movements could be observed to initiate from actin patches, suggesting cable assembly from the patches (Figure 6G). We conclude that, independent of the specific formin, CP insulates actin patches from formins, restricting their activity to the proper location.

DISCUSSION

How cells simultaneously assemble functionally diverse actin structures of distinct identity within a common cytosol is a debated question. Arp2/3 and formins, respectively, assemble branched and linear actin structures decorated by largely distinct actin-binding proteins. A hallmark of formins is their ability to promote barbed-end growth against the growth-arrest function of CP, a feature demonstrated in numerous *in vitro* studies [27–32]. However, how CP may prevail against formins *in vivo* was largely unexplored. Here, we have shown that CP protects Arp2/3-assembled actin patches against formins, thus preserving their identity and restricting formins to their proper location.

Our interest in CP arose from the cell-fusion delay of *acp2Δ* cells. For fusion, cells locally digest their cell wall by concentrating the exocytosis of secretory vesicles containing cell-wall hydrolase at the site of cell-cell contact [42]. In WT cells, this is achieved by the Fus1-assembled actin fusion focus. By contrast, in cells lacking CP, despite strong Fus1 accumulation at the fusion site, secretory vesicles are frequently diverted away from the fusion site to ectopic Fus1 foci at actin patches. This correlates with a reduction in secretory vesicles at the fusion focus, which likely explains the fusion delay. Indeed, the forced diversion of Myo52 to actin patches also yields extended fusion times. Thus, the fusion defect of CP mutants likely results from diversion of secretory vesicles to ectopic sites, rather than from excessive actin assembly at the fusion site. Because CP mutants exhibit longer actin patch lifetimes [24], which may lead to slower endocytosis, the fusion delay may also partly result from reduced recycling of the pheromone receptor from the plasma membrane [58].

This raises the question of where CP acts—in formin-assembled structures or at Arp2/3-assembled patches. We argue that the formin-CP competition happens throughout the cell, with distinct outcomes: in formin-assembled structures, the formin wins and CP is largely dispensable; at actin patches, CP dominates and insulates this structure against formins. These distinct outcomes are reflected in the exclusive localization of CP at patches and restriction of formins to other cellular locations. The occasional ectopic foci detected in WT cells illustrate that CP patch protection against formins is an active process that can transiently fail even in WT cells.

CP-formin competition is best revealed by alteration of Fus1 and/or CP function. At the fusion focus, the competition is exposed by Fus1 FH2 mutations. A first observation is that FH2 mutations compromise fusion to various extents *in vivo*, although they all fully abrogated actin assembly *in vitro* [51]. The poor predictive value of the *in vitro* activity may be due to high local Fus1 concentration in the focus, which likely exceeds the concentrations tested *in vitro*. A second observation is the strong allele-specific suppression by *acp2Δ* of the fusion defect of $fus1^{I951A}$, which carries a mutation in the knob. This allele-specific suppression is consistent with the proposed structural arrangement of the formin-CP ternary complex at the barbed end, which shows a steric clash between the formin knob and CPβ [31]. The I951A mutation likely favors the binding of CPβ, thus promoting capping function in the ternary complex, which is relieved upon CPβ deletion. In the cell, the inability of $Fus1^{I951A}$ to assemble a fusion focus must be due to CP competing with the formin at the fusion site. Further evidence for competition at this location comes from increased Fus1 intensity at the fusion focus and the extended focus lifetime in CP mutants. This suggests that small amounts (below detection levels) of CP may compete with Fus1 in the fusion focus, although the increased Fus1 intensity may also be due to Fus1 recruitment to adjacent patches. We conclude that some Fus1-CP competition can take place at the fusion site, where Fus1 normally dominates.

Our data indicate that the principal sites of formin-CP competition are actin patches, where CP efficiently outcompetes Fus1. In WT cells, CP is strongly enriched at actin patches and prevents formin binding. In cells lacking CP function, all three formins localize to actin patches. The strength of CP protection against formins largely scales with its barbed-end binding affinity as measured *in vitro* [14], with $acp2^{\Delta t}$ showing fewer ectopic foci than $acp1^{\Delta t}$, and *acp1Δ* or *acp2Δ*. When CP is absent from patches, these acquire characteristics of linear actin structures: they are decorated by myosin V Myo51 and tropomyosin, which normally preferentially associate with actin cables, ring, and focus [7, 44, 45, 48–50, 52, 53]; they also accumulate the myosin V Myo52, which erroneously transports its cargoes to these locations. The coincidence of tropomyosin and fimbrin at patches devoid of CP is striking given recent findings that competition between these actin-binding proteins drives their specific association with formin- and Arp2/3-assembled structure *in vitro*, respectively [9–11]. Importantly, For3 is absent from tropomyosin-decorated *fim1Δ* patches, indicating that formins localize to patches because of a specific defect in capping rather than a global change in actin cytoskeleton homeostasis. We conclude that, in the absence of CP, actin patches acquire a double identity.

One important question is whether the double identity of CP-devoid patches arises from ectopic formin activity or simply from uncapping. This question is difficult to address because

any perturbation in actin structures will perturb homeostasis [3]. For instance, formin deletion frees G-actin and tropomyosin, which now incorporate in actin patches. Conversely, actin patch disruption enhances formin-assembled structures, now more permissive for fimbrin association. However, two observations argue for formin activity at CP-devoid patches. First, during mating, Myo52 was not present at all actin patches, but was always there when Fus1 was. This argues that Fus1 activity is the driving force for vesicular cargo recruitment. Second, the For3 flow from patches indicates assembly of cables from this location [47]. As a side note, although the mechanism and function of For3 retrograde flow remain unknown, it occurred, and at similar rates, in *acp2Δ* cells, indicating that flow is not due to arrest of For3-dependent filament elongation upon formation of a ternary formin-CP complex. Together, these observations indicate that patch-localized formins actively assemble linear actin filaments.

An interesting observation is that *acp2Δ* cells consistently displayed stronger phenotypes not only than *acp1Δ* but also than *acp1Δ acp2Δ* double mutants. Berro and Pollard also previously noted that the phenotypes of *acp2Δ* and *acp1Δ* are not identical [24]. We note that our data show a quantitative, but not qualitative, difference between these genotypes. It is formally possible that the stronger phenotype of *acp2Δ* cells is due to a CPβ function partly unrelated to capping activity. However, the weaker phenotype of *acp1Δ acp2Δ* instead indicates that Acp1 not bound by Acp2 enhances the phenotype. One interpretation is that, although formins gain access to actin barbed ends in the absence of Acp2, they may gain better access if Acp1 is still present. Because Acp1 still weakly binds the actin barbed end in the absence of Acp2 *in vitro* [16], its presence may somehow help recruit formins to the barbed end. This interpretation predicts an interaction between formins and CPα, a hypothesis consistent with human INF2 formin association with CPα [59].

Because CP-formin competition yields distinct outcomes at the sites of formin action and Arp2/3-assembled patches, one question is what defines the competition outcome. Part of the answer comes from the $Acp2^{R12A,Y77A}$ allele, carrying mutations in the CPI-binding residues, which compromises CP localization to actin patches. This finding agrees with previous data in human cells that CP localization relies on interaction with CPI-containing proteins [18]. The specific CP-binding partners are unknown in *S. pombe*, but may involve the homolog of *S. cerevisiae* Aim21, which binds CP through the CPI-binding residues and contributes to its localization to actin patches [19], although this finding was not reproduced in a second study [20]. Consistent with this hypothesis, deletion of *S. pombe* Aim21 was identified in our genome-wide screen to have fusion defects [45]. The phenotype of $acp2^{R12A,Y77A}$ cells indicates that CP recruitment to actin patches by pre-localized partners is required to protect them against formin activity. Thus, barbed-end-independent recruitment of CP may tip the CP-formin competition in favor of CP in Arp2/3-assembled structures.

The findings described in our study present the CP-formin competition in a new light, where CP protects Arp2/3 structures against ectopic localization of formins. In fission yeast *acp2Δ* cells, formin localization to actin patches has important consequences for cellular organization: during mating, Fus1 diverts cargoes away from the fusion site, slowing the fusion process; in interphase cells, For3 activity at patches may cause the previously noted actin cable disorganization and partial loss of cell polarity, leading to actin patch depolarization [24, 33]; in dividing cells, the reason for the cytokinetic defect of cells lacking CP [33] may also be the titration of Cdc12 to actin patches. Because CP is ubiquitous in eukaryotic cells, it likely protects the identity of Arp2/3 actin assemblies and prevents formin ectopic activity in a vast range of organisms.

STAR★METHODS

Detailed methods are provided in the online version of this paper and include the following:

- KEY RESOURCES TABLE
- LEAD CONTACT AND MATERIALS AVAILABILITY
- EXPERIMENTAL MODEL AND SUBJECT DETAILS
- METHOD DETAILS
  - Strain Construction
  - Mating Assays
  - Microscopy
- QUANTIFICATION AND STATISTICAL ANALYSIS
- DATA AND CODE AVAILABILITY

SUPPLEMENTAL INFORMATION

Supplemental Information can be found online at https://doi.org/10.1016/j.cub.2019.07.088.

ACKNOWLEDGMENTS

We thank Dr. David Kovar (University of Chicago) for strains, Dr. Aleksandar Vjestica for plasmids, Dr. Omaya Dudin for initial guidance and supervision, Dr. Magdalena Marek for strains, and Dr. Laura Merlini, Dr. Olivia Muriel Lopez, and Dr. Veneta Gerganova for comments on the manuscript. This work was supported by an ERC consolidator grant (CellFusion) and a Swiss National Science Foundation grant (310030B_176396) (to S.G.M.).

AUTHOR CONTRIBUTIONS

I.B.-C. performed all experiments; I.B.-C. made the figures, with contributions from S.G.M.; I.B.-C. and S.G.M. wrote the manuscript; S.G.M. provided supervision; and S.G.M. acquired funding.

DECLARATION OF INTERESTS

The authors declare no competing interests.

Received: May 22, 2019
Revised: July 4, 2019
Accepted: July 30, 2019
Published: September 5, 2019

REFERENCES

1. Kovar, D.R., Sirotkin, V., and Lord, M. (2011). Three's company: the fission yeast actin cytoskeleton. Trends Cell Biol. *21*, 177–187.
2. Campellone, K.G., and Welch, M.D. (2010). A nucleator arms race: cellular control of actin assembly. Nat. Rev. Mol. Cell Biol. *11*, 237–251.
3. Burke, T.A., Christensen, J.R., Barone, E., Suarez, C., Sirotkin, V., and Kovar, D.R. (2014). Homeostatic actin cytoskeleton networks are regulated by assembly factor competition for monomers. Curr. Biol. *24*, 579–585.

4. Suarez, C., Carroll, R.T., Burke, T.A., Christensen, J.R., Bestul, A.J., Sees, J.A., James, M.L., Sirotkin, V., and Kovar, D.R. (2015). Profilin regulates F-actin network homeostasis by favoring formin over Arp2/3 complex. Dev. Cell *32*, 43–53.
5. Rotty, J.D., Wu, C., Haynes, E.M., Suarez, C., Winkelman, J.D., Johnson, H.E., Haugh, J.M., Kovar, D.R., and Bear, J.E. (2015). Profilin-1 serves as a gatekeeper for actin assembly by Arp2/3-dependent and -independent pathways. Dev. Cell *32*, 54–67.
6. Papp, G., Bugyi, B., Ujfalusi, Z., Barkó, S., Hild, G., Somogyi, B., and Nyitrai, M. (2006). Conformational changes in actin filaments induced by formin binding to the barbed end. Biophys. J. *91*, 2564–2572.
7. Skau, C.T., Neidt, E.M., and Kovar, D.R. (2009). Role of tropomyosin in formin-mediated contractile ring assembly in fission yeast. Mol. Biol. Cell *20*, 2160–2173.
8. Johnson, M., East, D.A., and Mulvihill, D.P. (2014). Formins determine the functional properties of actin filaments in yeast. Curr. Biol. *24*, 1525–1530.
9. Christensen, J.R., Hocky, G.M., Homa, K.E., Morganthaler, A.N., Hitchcock-DeGregori, S.E., Voth, G.A., and Kovar, D.R. (2017). Competition between tropomyosin, fimbrin, and ADF/cofilin drives their sorting to distinct actin filament networks. eLife *6*, e23152.
10. Clayton, J.E., Sammons, M.R., Stark, B.C., Hodges, A.R., and Lord, M. (2010). Differential regulation of unconventional fission yeast myosins via the actin track. Curr. Biol. *20*, 1423–1431.
11. Skau, C.T., and Kovar, D.R. (2010). Fimbrin and tropomyosin competition regulates endocytosis and cytokinesis kinetics in fission yeast. Curr. Biol. *20*, 1415–1422.
12. Edwards, M., Zwolak, A., Schafer, D.A., Sept, D., Dominguez, R., and Cooper, J.A. (2014). Capping protein regulators fine-tune actin assembly dynamics. Nat. Rev. Mol. Cell Biol. *15*, 677–689.
13. Yamashita, A., Maeda, K., and Maéda, Y. (2003). Crystal structure of CapZ: structural basis for actin filament barbed end capping. EMBO J. *22*, 1529–1538.
14. Wear, M.A., Yamashita, A., Kim, K., Maéda, Y., and Cooper, J.A. (2003). How capping protein binds the barbed end of the actin filament. Curr. Biol. *13*, 1531–1537.
15. Narita, A., Takeda, S., Yamashita, A., and Maéda, Y. (2006). Structural basis of actin filament capping at the barbed-end: a cryo-electron microscopy study. EMBO J. *25*, 5626–5633.
16. Kim, K., Yamashita, A., Wear, M.A., Maéda, Y., and Cooper, J.A. (2004). Capping protein binding to actin in yeast: biochemical mechanism and physiological relevance. J. Cell Biol. *164*, 567–580.
17. Hernandez-Valladares, M., Kim, T., Kannan, B., Tung, A., Aguda, A.H., Larsson, M., Cooper, J.A., and Robinson, R.C. (2010). Structural characterization of a capping protein interaction motif defines a family of actin filament regulators. Nat. Struct. Mol. Biol. *17*, 497–503.
18. Edwards, M., McConnell, P., Schafer, D.A., and Cooper, J.A. (2015). CPI motif interaction is necessary for capping protein function in cells. Nat. Commun. *6*, 8415.
19. Farrell, K.B., McDonald, S., Lamb, A.K., Worcester, C., Peersen, O.B., and Di Pietro, S.M. (2017). Novel function of a dynein light chain in actin assembly during clathrin-mediated endocytosis. J. Cell Biol. *216*, 2565–2580.
20. Shin, M., van Leeuwen, J., Boone, C., and Bretscher, A. (2018). Yeast Aim21/Tda2 both regulates free actin by reducing barbed end assembly and forms a complex with Cap1/Cap2 to balance actin assembly between patches and cables. Mol. Biol. Cell *29*, 923–936.
21. Akin, O., and Mullins, R.D. (2008). Capping protein increases the rate of actin-based motility by promoting filament nucleation by the Arp2/3 complex. Cell *133*, 841–851.
22. Iwasa, J.H., and Mullins, R.D. (2007). Spatial and temporal relationships between actin-filament nucleation, capping, and disassembly. Curr. Biol. *17*, 395–406.
23. Mejillano, M.R., Kojima, S., Applewhite, D.A., Gertler, F.B., Svitkina, T.M., and Borisy, G.G. (2004). Lamellipodial versus filopodial mode of the actin nanomachinery: pivotal role of the filament barbed end. Cell *118*, 363–373.
24. Berro, J., and Pollard, T.D. (2014). Synergies between Aip1p and capping protein subunits (Acp1p and Acp2p) in clathrin-mediated endocytosis and cell polarization in fission yeast. Mol. Biol. Cell *25*, 3515–3527.
25. Kaksonen, M., Toret, C.P., and Drubin, D.G. (2005). A modular design for the clathrin- and actin-mediated endocytosis machinery. Cell *123*, 305–320.
26. Kim, K., Galletta, B.J., Schmidt, K.O., Chang, F.S., Blumer, K.J., and Cooper, J.A. (2006). Actin-based motility during endocytosis in budding yeast. Mol. Biol. Cell *17*, 1354–1363.
27. Zigmond, S.H., Evangelista, M., Boone, C., Yang, C., Dar, A.C., Sicheri, F., Forkey, J., and Pring, M. (2003). Formin leaky cap allows elongation in the presence of tight capping proteins. Curr. Biol. *13*, 1820–1823.
28. Kovar, D.R., Kuhn, J.R., Tichy, A.L., and Pollard, T.D. (2003). The fission yeast cytokinesis formin Cdc12p is a barbed end actin filament capping protein gated by profilin. J. Cell Biol. *161*, 875–887.
29. Moseley, J.B., Sagot, I., Manning, A.L., Xu, Y., Eck, M.J., Pellman, D., and Goode, B.L. (2004). A conserved mechanism for Bni1- and mDia1-induced actin assembly and dual regulation of Bni1 by Bud6 and profilin. Mol. Biol. Cell *15*, 896–907.
30. Harris, E.S., Li, F., and Higgs, H.N. (2004). The mouse formin, FRLalpha, slows actin filament barbed end elongation, competes with capping protein, accelerates polymerization from monomers, and severs filaments. J. Biol. Chem. *279*, 20076–20087.
31. Shekhar, S., Kerleau, M., Kühn, S., Pernier, J., Romet-Lemonne, G., Jégou, A., and Carlier, M.F. (2015). Formin and capping protein together embrace the actin filament in a ménage à trois. Nat. Commun. *6*, 8730.
32. Bombardier, J.P., Eskin, J.A., Jaiswal, R., Corrêa, I.R., Jr., Xu, M.Q., Goode, B.L., and Gelles, J. (2015). Single-molecule visualization of a formin-capping protein 'decision complex' at the actin filament barbed end. Nat. Commun. *6*, 8707.
33. Kovar, D.R., Wu, J.Q., and Pollard, T.D. (2005). Profilin-mediated competition between capping protein and formin Cdc12p during cytokinesis in fission yeast. Mol. Biol. Cell *16*, 2313–2324.
34. Sinnar, S.A., Antoku, S., Saffin, J.M., Cooper, J.A., and Halpain, S. (2014). Capping protein is essential for cell migration in vivo and for filopodial morphology and dynamics. Mol. Biol. Cell *25*, 2152–2160.
35. Bear, J.E., and Gertler, F.B. (2009). Ena/VASP: towards resolving a pointed controversy at the barbed end. J. Cell Sci. *122*, 1947–1953.
36. Martin, S.G. (2016). Role and organization of the actin cytoskeleton during cell-cell fusion. Semin. Cell Dev. Biol. *60*, 121–126.
37. Kaksonen, M., Sun, Y., and Drubin, D.G. (2003). A pathway for association of receptors, adaptors, and actin during endocytic internalization. Cell *115*, 475–487.
38. Sirotkin, V., Berro, J., Macmillan, K., Zhao, L., and Pollard, T.D. (2010). Quantitative analysis of the mechanism of endocytic actin patch assembly and disassembly in fission yeast. Mol. Biol. Cell *21*, 2894–2904.
39. Aghamohammadzadeh, S., and Ayscough, K.R. (2009). Differential requirements for actin during yeast and mammalian endocytosis. Nat. Cell Biol. *11*, 1039–1042.
40. Amatruda, J.F., and Cooper, J.A. (1992). Purification, characterization, and immunofluorescence localization of *Saccharomyces cerevisiae* capping protein. J. Cell Biol. *117*, 1067–1076.
41. Nakano, K., and Mabuchi, I. (2006). Actin-capping protein is involved in controlling organization of actin cytoskeleton together with ADF/cofilin, profilin and F-actin crosslinking proteins in fission yeast. Genes Cells *11*, 893–905.
42. Dudin, O., Bendezú, F.O., Groux, R., Laroche, T., Seitz, A., and Martin, S.G. (2015). A formin-nucleated actin aster concentrates cell wall hydrolases for cell fusion in fission yeast. J. Cell Biol. *208*, 897–911.
43. Petersen, J., Weilguny, D., Egel, R., and Nielsen, O. (1995). Characterization of fus1 of *Schizosaccharomyces pombe*: a developmentally controlled function needed for conjugation. Mol. Cell. Biol. *15*, 3697–3707.

44. Kurahashi, H., Imai, Y., and Yamamoto, M. (2002). Tropomyosin is required for the cell fusion process during conjugation in fission yeast. Genes Cells *7*, 375–384.

45. Dudin, O., Merlini, L., Bendezú, F.O., Groux, R., Vincenzetti, V., and Martin, S.G. (2017). A systematic screen for morphological abnormalities during fission yeast sexual reproduction identifies a mechanism of actin aster formation for cell fusion. PLoS Genet. *13*, e1006721.

46. Karagiannis, J., Bimbó, A., Rajagopalan, S., Liu, J., and Balasubramanian, M.K. (2005). The nuclear kinase Lsk1p positively regulates the septation initiation network and promotes the successful completion of cytokinesis in response to perturbation of the actomyosin ring in *Schizosaccharomyces pombe*. Mol. Biol. Cell *16*, 358–371.

47. Martin, S.G., and Chang, F. (2006). Dynamics of the formin for3p in actin cable assembly. Curr. Biol. *16*, 1161–1170.

48. Balasubramanian, M.K., Helfman, D.M., and Hemmingsen, S.M. (1992). A new tropomyosin essential for cytokinesis in the fission yeast *S. pombe*. Nature *360*, 84–87.

49. Arai, R., Nakano, K., and Mabuchi, I. (1998). Subcellular localization and possible function of actin, tropomyosin and actin-related protein 3 (Arp3) in the fission yeast *Schizosaccharomyces pombe*. Eur. J. Cell Biol. *76*, 288–295.

50. Coulton, A.T., East, D.A., Galinska-Rakoczy, A., Lehman, W., and Mulvihill, D.P. (2010). The recruitment of acetylated and unacetylated tropomyosin to distinct actin polymers permits the discrete regulation of specific myosins in fission yeast. J. Cell Sci. *123*, 3235–3243.

51. Scott, B.J., Neidt, E.M., and Kovar, D.R. (2011). The functionally distinct fission yeast formins have specific actin-assembly properties. Mol. Biol. Cell *22*, 3826–3839.

52. Wang, N., Lo Presti, L., Zhu, Y.H., Kang, M., Wu, Z., Martin, S.G., and Wu, J.Q. (2014). The novel proteins Rng8 and Rng9 regulate the myosin-V Myo51 during fission yeast cytokinesis. J. Cell Biol. *205*, 357–375.

53. Lo Presti, L., Chang, F., and Martin, S.G. (2012). Myosin Vs organize actin cables in fission yeast. Mol. Biol. Cell *23*, 4579–4591.

54. Wu, J.Q., Bähler, J., and Pringle, J.R. (2001). Roles of a fimbrin and an alpha-actinin-like protein in fission yeast cell polarization and cytokinesis. Mol. Biol. Cell *12*, 1061–1077.

55. Skau, C.T., Courson, D.S., Bestul, A.J., Winkelman, J.D., Rock, R.S., Sirotkin, V., and Kovar, D.R. (2011). Actin filament bundling by fimbrin is important for endocytosis, cytokinesis, and polarization in fission yeast. J. Biol. Chem. *286*, 26964–26977.

56. Sizonenko, G.I., Karpova, T.S., Gattermeir, D.J., and Cooper, J.A. (1996). Mutational analysis of capping protein function in *Saccharomyces cerevisiae*. Mol. Biol. Cell *7*, 1–15.

57. Chang, F. (1999). Movement of a cytokinesis factor cdc12p to the site of cell division. Curr. Biol. *9*, 849–852.

58. Dudin, O., Merlini, L., and Martin, S.G. (2016). Spatial focalization of pheromone/MAPK signaling triggers commitment to cell-cell fusion. Genes Dev. *30*, 2226–2239.

59. Rollason, R., Wherlock, M., Heath, J.A., Heesom, K.J., Saleem, M.A., and Welsh, G.I. (2016). Disease causing mutations in inverted formin 2 regulate its binding to G-actin, F-actin capping protein (CapZ α-1) and profilin 2. Biosci. Rep. *36*, e00302.

60. Bähler, J., Wu, J.Q., Longtine, M.S., Shah, N.G., McKenzie, A., III, Steever, A.B., Wach, A., Philippsen, P., and Pringle, J.R. (1998). Heterologous modules for efficient and versatile PCR-based gene targeting in *Schizosaccharomyces pombe*. Yeast *14*, 943–951.

61. Egel, R., Willer, M., Kjaerulff, S., Davey, J., and Nielsen, O. (1994). Assessment of pheromone production and response in fission yeast by a halo test of induced sporulation. Yeast *10*, 1347–1354.

62. Vjestica, A., Merlini, L., Dudin, O., Bendezu, F.O., and Martin, S.G. (2016). Microscopy of fission yeast sexual lifecycle. J. Vis. Exp. *109*, 10.3791/53801.

63. Cheng, H., Sugiura, R., Wu, W., Fujita, M., Lu, Y., Sio, S.O., Kawai, R., Takegawa, K., Shuntoh, H., and Kuno, T. (2002). Role of the Rab GTP-binding protein Ypt3 in the fission yeast exocytic pathway and its connection to calcineurin function. Mol. Biol. Cell *13*, 2963–2976.

64. Skoumpla, K., Coulton, A.T., Lehman, W., Geeves, M.A., and Mulvihill, D.P. (2007). Acetylation regulates tropomyosin function in the fission yeast *Schizosaccharomyces pombe*. J. Cell Sci. *120*, 1635–1645.

STAR★METHODS

KEY RESOURCES TABLE

REAGENT or RESOURCE	SOURCE	IDENTIFIER
Chemicals, Peptides, and Recombinant Proteins		
LatrunculinA	Enzo Life Science	Cat# T-119-0500
CK666	Sigma	Cat# SML0006
AgaPure Agarose LE	Canvax	Cat# AG006
Vaselin	Reactolab	Cat# 99813
Lanolin	Sigma	Cat# L7387
Paraffin	Reactolab	Cat# 99756
Dimethyl sulfoxide (DMSO)	Applichem	Cat# 1584
Poly(ethylene glycol) BioUltra, 4,000	Sigma	Cat# 95904
Lithium Acetat Dihydrat	Applichem	Cat# A3478
EDTA Disodium Salt 2-hydrate	Applichem	Cat# A2937
Tris(hydroxymethyl)aminomethane	Biosolve	Cat# 200923
Experimental Models: Organisms/Strains		
h90 myo52-tdTomato:natMX ura4-294:p^{map3}-GFP:ura4+	Lab Stock	YSM2535
h90 myo52-tdTomato:natMX ura4-294:p^{map3}-GFP-ura4+ acp1::kanMX	Lab Stock	YSM3307
h90 myo52-tdTomato:natMX ura4-294:p^{map3}-GFP-ura4+ acp2::kanMX	Lab Stock	YSM2955
h90 myo52-tdTomato:natMX ura4-294:p^{map3}-GFP-ura4+ acp1::kanMX acp2::kanMX	This work	YSM3308
h90 myo52-tdTomato:natMX leu1-32:p^{nmt41}-GFP-CHD:leu1^{+}	Lab Stock	YSM2515
h90 myo52-tdTomato:natMX leu1-32:p^{nmt41}-GFP-CHD:leu1^{+} acp1::hphMX	This work	YSM3309
h90 myo52-tdTomato:natMX leu1-32:p^{nmt41}-GFP-CHD:leu1^{+} acp2::bleMX	This work	YSM3310
h90 myo52-tdTomato:natMX leu1-32:p^{nmt41}-GFP-CHD:leu1^{+} acp1::hphMX acp2::bleMX	This work	YSM3311
h90 myo52-tdTomato:natMX fus1-sfGFP:kanMX	This work	YSM3312
h90 myo52-tdTomato:natMX fus1-sfGFP:kanMX acp1::hphMX	This work	YSM3313
h90 myo52-tdTomato:natMX fus1-sfGFP:kanMX acp2::bleMX	This work	YSM3314
h90 myo52-tdTomato:natMX fus1-sfGFP:kanMX acp1::hphMX acp2::bleMX	This work	YSM3315
h90 myo52-tdTomato:natMX leu1::p^{nmt41}-GFP-cdc8:ura4^{+}	This work	YSM3316
h90 myo52-tdTomato:natMX leu1::p^{nmt41}-GFP-cdc8:ura4^{+} acp2::bleMX	This work	YSM3317
h90 myo52-tdTomato:natMX fus1^{K879A}-sfGFP:kanMX	This work	YSM3318
h90 myo52-tdTomato:natMX fus1^{I951A}-sfGFP:kanMX	This work	YSM3319
h90 myo52-tdTomato:natMX fus1^{GN1087,1088RP}-sfGFP:kanMX	This work	YSM3320
h90 myo52-tdTomato:natMX fus1^{K1112A}-sfGFP:kanMX	This work	YSM3321
h90 myo52-tdTomato:natMX fus1^{K879A}-sfGFP:kanMX acp2::bleMX	This work	YSM3322
h90 myo52-tdTomato:natMX fus1^{I951A}-sfGFP:kanMX acp2::bleMX	This work	YSM3323
h90 myo52-tdTomato:natMX fus1^{GN1087,1088RP}-sfGFP:kanMX acp2::bleMX	This work	YSM3324
h90 myo52-tdTomato:natMX fus1^{K1112A}-sfGFP:kanMX acp2::bleMX	This work	YSM3325
h90 myo52-tdTomato:natMX acp2-sfGFP:kanMX fus1::hphMX	This work	YSM3433
h90 myo52-tdTomato:natMX ura4-294:p^{nmt1}-fus1-sfGFP:ura4^{+}	This work	YSM3328
h90 myo52-tdTomato:natMX exo84-GFP:kanMX	This work	YSM3329
h90 myo52-tdTomato:natMX exo84-GFP:kanMX acp1::hphMX	This work	YSM3330
h90 myo52-tdTomato:natMX exo84-GFP:kanMX acp2::bleMX	This work	YSM3331
h90 myo52-tdTomato:natMX exo84-GFP:kanMX acp1::hphMX acp2::bleMX	This work	YSM3332
h90 myo52-tdTomato:natMX exo70-GFP:kanMX	This work	YSM3333

(*Continued on next page*)

Continued

REAGENT or RESOURCE	SOURCE	IDENTIFIER
h90 myo52-tdTomato:natMX exo70-GFP:kanMX acp1::hphMX	This work	YSM3334
h90 myo52-tdTomato:natMX exo70-GFP:kanMX acp2::bleMX	This work	YSM3335
h90 myo52-tdTomato:natMX exo70-GFP:kanMX acp1::hphMX acp2::bleMX	This work	YSM3336
h90 myo52-tdTomato:natMX ura4-294:p^{nmt41}-GFP-ypt3:ura4^{+}	This work	YSM3337
h90 myo52-tdTomato:natMX ura4-294:p^{nmt41}-GFP-ypt3:ura4^{+} acp1::hphMX	This work	YSM3338
h90 myo52-tdTomato:natMX ura4-294:p^{nmt41}-GFP-ypt3:ura4^{+} acp2::bleMX	This work	YSM3339
h90 myo52-tdTomato:natMX ura4-294:p^{nmt41}-GFP-ypt3:ura4^{+} acp1::hphMX acp2::bleMX	This work	YSM3340
h90 myo52-tdTomato:natMX agn2-sfGFP:kanMX	Lab Stock	YSM2571
h90 myo52-tdTomato:natMX agn2-sfGFP:kanMX acp1::hphMX	This work	YSM3341
h90 myo52-tdTomato:natMX agn2-sfGFP:kanMX acp2::bleMX	This work	YSM3342
h90 myo52-tdTomato:natMX agn2-sfGFP:kanMX acp1::hphMX acp2::bleMX	This work	YSM3343
h90 myo52-tdTomato:natMX eng2-sfGFP:kanMX	Lab Stock	YSM2572
h90 myo52-tdTomato:natMX eng2-sfGFP:kanMX acp1::hphMX	This work	YSM3344
h90 myo52-tdTomato:natMX eng2-sfGFP:kanMX acp2::bleMX	This work	YSM3345
h90 myo52-tdTomato:natMX eng2-sfGFP:kanMX acp1::hphMX acp2::bleMX	This work	YSM3346
h90 myo52-tdTomato:natMX	Lab Stock	YSM2440
h90 myo52-tdTomato:natMX myo51-sfGFP:kanMX	This work	YSM3347
h90 myo52-tdTomato:natMX myo51-sfGFP:kanMX acp2::bleMX	This work	YSM3348
h90 fim1-mCherry:natMX fus1-sfGFP:kanMX	This work	YSM3349
h90 fim1-mCherry:natMX fus1-sfGFP:kanMX acp2::bleMX	This work	YSM3350
h90 fim1-mCherry:natMX myo51-sfGFP:kanMX	This work	YSM3351
h90 fim1-mCherry:natMX myo51-sfGFP:kanMX acp2::bleMX	This work	YSM3352
h90 myo52-tdTomato:natMX acp1$^{\Delta tentacle}$-sfGFP:kanMX	This work	YSM3353
h90 myo52-tdTomato:natMX acp1-sfGFP:kanMX acp2::bleMX	This work	YSM3354
h90 myo52-tdTomato:natMX acp2-sfGFP:kanMX	This work	YSM3355
h90 myo52-tdTomato:natMX acp2$^{\Delta tentacle}$-sfGFP:kanMX	This work	YSM3356
h90 myo52-tdTomato:natMX acp2-sfGFP-kanMX acp1::hphMX	This work	YSM3357
h90 myo52-tdTomato:natMX acp2^{R12A,Y77A}-sfGFP:kanMX	This work	YSM3358
h90 myo52-GFP:kanMX	Lab Stock	YSM2520
h90 myo52-GFP:kanMX fim1-GBP-mCherry:kanMX	This work	YSM3359
h90 myo52-tdTomato:natMX fim1-sfGFP:kanMX	This work	YSM3360
h90 myo52-tdTomato:natMX fim1-sfGFP:kanMX acp2::bleMX	This work	YSM3361
h90 fim1-mCherry:natMX leu1::p^{nmt41}-GFP-cdc8:ura4^{+}	This work	YSM3362
h90 fim1-mCherry:natMX leu1::p^{nmt41}-GFP-cdc8:ura4^{+} acp2::bleMX	This work	YSM3363
h90 fim1-mCherry:natMX for3-3GFP:ura4^{+}	This work	YSM3364
h90 fim1-mCherry:natMX for3-3GFP:ura4^{+} acp2::bleMX	This work	YSM3365
h+ fim1-mCherry:natMX cdc12-3GFP:ura4^{+}	This work	YSM3366
h+ fim1-mCherry:natMX cdc12-3GFP:ura4^{+} acp2::bleMX	This work	YSM3367
h- leu1-32:p^{act1}-LifeAct-mCherry:leu1^{+}	Lab Stock	YSM3434
h- leu1-32:p^{act1}-LifeAct-mCherry:leu1^{+} acp2^{R12A,Y77A}-sfGFP:kanMX	This work	YSM3435
h- leu1-32:p^{act1}-LifeAct-mCherry:leu1^{+} acp1$^{\Delta tentacle}$-sfGFP:kanMX	This work	YSM3436
h- leu1-32:p^{act1}-LifeAct-mCherry:leu1^{+} acp2$^{\Delta tentacle}$-sfGFP:kanMX	This work	YSM3437
h- fim1-mCherry:natMX leu1::p^{nmt41}-GFP-cdc8:ura4+ for3::bsd	This work	YSM3368
h- fim1-mCherry:natMX leu1::p^{nmt41}-GFP-cdc8:ura4+ for3::bsd acp2::bleMX	This work	YSM3369
h- fim1-mCherry:natMX leu1::p^{nmt41}-GFP-cdc8:ura4+ for3::kanMX cdc12-112	This work	YSM3370
h- fim1-mCherry:natMX leu1::p^{nmt41}-GFP-cdc8:ura4+ for3::kanMX cdc12-112 acp2::bleMX	This work	YSM3371

(*Continued on next page*)

Continued		
REAGENT or RESOURCE	SOURCE	IDENTIFIER
h90 for3-3GFP:ura4⁺ acp2-mCherry:natMX	This work	YSM3438
h90 for3-3GFP:ura4⁺ acp2-mCherry:natMX fim1::bleMX	This work	YSM3439
Oligonucleotides		
Primers for PCR, see Table S1	This work	N/A
Recombinant DNA		
pFA6a vector	[60]	pSM644
pFA6a-sfGFP-kanMX *(to generate Myo51-sfGFP, Fim1-sfGFP, acp1-sfGFP, acp1$^{\Delta t}$-sfGFP, acp2-sfGFP and acp2$^{\Delta t}$-sfGFP)*	Lab Stock	pSM1538
pFA6a-mCherry-natMX *(to generate Fim1-mCherry and Acp2-mCherry)*	Lab Stock	pSM684
pFA6a-GBP-mCherry-natMX *(to generate Fim1-GBP-mCherry)*	Lab Stock	pSM1768
pFA6a-hphMX *(to generate acp1Δ)*	Lab Stock	pSM693
pFA6a-bleMX *(to generate acp2Δ)*	Lab Stock	pSM694
pSP72 vector	Promega	pSM1232
pSP72-5′UTR-acp2-sfGFP-kanMX-3′UTR	This work	pSM2194
pSP72-5′UTR-acp2^{R12A}-sfGFP-kanMX-3′UTR	This work	pSM2201
pSP72-5′UTR-acp2^{R12AY77A}-sfGFP-kanMX-3′UTR	This work	pSM2203
pSP72-5′UTR-fus1-sfGFP-kanMX-3′UTR	This work	pSM2218
pSP72-5′UTR-fus1^{K879A}-sfGFP-kanMX-3′UTR	This work	pSM2251
pSP72-5′UTR-fus1^{I951A}-sfGFP-kanMX-3′UTR	This work	pSM2252
pSP72-5′UTR-fus1^{GN1087,1088RP}-sfGFP-kanMX-3′UTR	This work	pSM2253
pSP72-5′UTR-fus1^{K1112A}-sfGFP-kanMX-3′UTR	This work	pSM2254
pREP1 vector	Lab Stock	pSM1758
pUra4^{AfeI} vector	Lab Stock	pAV133
pUra4^{AfeI}-p^{nmt1}-fus1-sfGFP	This work	pSM2282
pREP41-GFP-ypt3	Lab Stock	pSM893
pUra4^{AfeI}-pnmt41-GFP-ypt3	This work	pSM2250
Software and Algorithms		
ImageJ (Fiji)	NIH	RRID: SCR_002285
S. pombe database (released in August, 2013)	PomBase	RRID: SCR_006586
Image Lab	Bio-Rad	RRID: SCR_014210
Volocity	PerkinElmer	RRID: SCR_002668
softWoRx v4.1.2	Applied Precision, GE Healthcare	No direct download
MATLAB	MathWorks	RRID: SCR_001622

LEAD CONTACT AND MATERIALS AVAILABILITY

Further information and requests for resources and reagents should be directed to and will be fulfilled by the Lead Contact, Sophie Martin (sophie.martin@unil.ch). Yeast strains generated in this study have not been deposited on an external repository but are available for distribution on request from the Lead Contact.

EXPERIMENTAL MODEL AND SUBJECT DETAILS

S. pombe strains used in this study are listed in the Key Resources Table. Homothallic (h90) strains able to switch mating types were used for all mating experiments, where cells were grown in liquid or agar Minimum Sporulation Media (MSL), with or without nitrogen (+/− N) [61, 62]. For interphase experiments, cells were grown in liquid or agar Edinburgh minimal medium (EMM) supplemented with amino acids as required.

METHOD DETAILS

Strain Construction

Strains were constructed using standard genetic manipulation of *S. pombe* either by tetrad dissection or transformation.

With two exceptions (*cdc8* and *ypt3*), genes were tagged at their endogenous genomic locus at their 3′ end, yielding C-terminally tagged proteins, or deleted by replacing their ORF by a resistance cassette. This was achieved by PCR amplification of a fragment from a template plasmid with primers carrying 5′ extensions corresponding to the last 78 coding nucleotides of the ORF (for C-terminal tagging) or the last 78 nucleotides of the 5′UTR (for gene deletion) and the first 78 nucleotides of the 3′UTR, which was transformed and integrated in the genome by homologous recombination, as previously described [60]. For tagging of genes with sfGFP, a pFA6a-sfGFP-kanMX plasmid (pSM1538) was used as a template for PCR-based targeted tagging of *myo51*, *fim1*, *acp1* and *acp2*. For tagging of genes with mCherry, a pFA6a-mCherry-natMX plasmid (pSM684) was used as a template for PCR-based targeted tagging of *fim1* and *acp2*. For tagging of genes with GBP-mCherry, a pFA6a-GBP-mCherry-natMX plasmid (pSM1768) was used as a template for PCR-based targeted tagging of *fim1*. For PCR-based targeted deletion, a pFA6a-hphMX plasmid (pSM693) or a pFA6a-bleMX plasmid (pSM694) was used as a template for *acp1* and *acp2* respectively. For deletion of the tentacle of Acp1 and Acp2, PCR-based targeted tagging was done using the last 78 nucleotides upstream of the C-terminal tentacle (R233-T256 for Acp1 and R244-I268 for Acp2). The functionality of the tagged proteins was verified by comparing the phenotype of the tagged strain with that of the deletion strain. For tagged Acp1 and Acp2 alleles, the number of ectopic foci was quantified and found to be as in wild-type cells. Reduced functionality was only observed for tagged Agn2 and Eng2 alleles, which in combination (but not individually) showed reduced fusion efficiency.

For point mutations of *acp2* (R12A-Y77A) and *fus1* (K879A, I951A, GN1087-1088RP, K1112A), a plasmid containing the full 5′UTR-ORF-sfGFP-kanMX-3′UTR sequence was first constructed by PCR amplification of the full fragment from strains YSM3312 or YSM3355 with primers carrying unique restriction sites, which were then cloned into a pSP72 plasmid (pSM1232). Site-directed mutagenesis was then conducted on these plasmids with primers containing the desired mutations. The resulting plasmids (pSM2203, pSM2251, pSM2252, pSM2253 and pSM2254, respectively) were sequenced, linearized and transformed into recipient strains YSM2440 for *acp2* and IBC178 (*fus1Δ* strain) for *fus1* mutants.

Construction of the strain overexpressing *fus1* (p^{nmt1}-fus1-sfGFP) was done by integration of fus1-sfGFP under the *nmt1* promoter at the *ura4+* locus. First, the *nmt1* promotor was amplified from a pREP1 plasmid (pSM1758) with primers carrying KpnI and NotI extensions. Second, the fus1-sfGFP fragment was amplified from strain YSM3312 with primers carrying NotI and SacI extensions. These two fragments were cloned by 3-point ligation into the vector pAV133 (pJK211, a kind gift from Dr. Aleksandar Vjestica, UNIL) digested with KpnI and SacI. The resulting plasmid (pSM2282) was sequenced, digested with AfeI and stably integrated as a single copy at the *ura4+* locus into strain YSM2440.

Construction of the strain expressing ypt3 (p^{nmt41}-GFP-ypt3) was done by integration of GFP-ypt3 under the *nmt41* promoter at the *ura4+* locus. The p^{nmt41}-GFP-ypt3 fragment was digested from a pREP41-GFP-ypt3 plasmid (pSM893) with PstI and XmaI and cloned into the vector pAV133 digested with the same enzymes. The resulting plasmid (pSM2250) was linearized by AfeI and transformed into strain YSM2440. This construct is in principle similar to that published by Cheng et al. [63], which was shown to rescue the *ypt3-i5* mutant phenotype. However, we note that we were unable to construct a GFP-ypt3 expressed as single copy from the native genomic locus, suggesting that GFP tagging impairs Ypt3 function.

The p^{nmt41}-GFP-cdc8 construct is integrated at the *leu1* locus and was shown to rescue the *cdc8-110* mutant phenotypes [64] (gratefully received from Prof David Kovar (Chicago University)). It is expressed in addition to the untagged *cdc8* gene copy at the endogenous genomic locus.

Mating Assays

Live imaging of *S. pombe* mating cells protocol was adapted from [62]. Briefly, cells were first pre-cultured overnight in MSL+N at 25°C, then diluted to OD_{600} = 0.05 into MSL+N at 25°C for 20 hours. Exponentially growing cells were then pelleted, washed in MSL-N by 3 rounds of centrifugation, and resuspended in MSL-N to an OD_{600} of 1.5. Cells were then grown 3 hours at 30°C to allow mating in liquid, added on 2% agarose MSL-N pads, and sealed with VALAP. We allowed the pads to rest for 30 min at 30°C before overnight imaging, or for 3 h before high speed imaging.

For interphase imaging, cells were grown to exponential phase at 30°C in EMM+ALU media, pelleted and added to 2% agarose EMM+ALU pads.

For CK-666 (Sigma) and LatA (Enzo Life Sciences) treatments, the drugs were added directly before imaging to the final resuspension, to a final concentration of 500μM and 200μM, respectively. In this case, cells were simply imaged without pad between slide and coverslip. The slide was allowed to rest for 5 minutes before imaging.

Microscopy

Images presented in Figures 1, 2, 3, 5, S2, S5C, and S5D, except Figure 2E were obtained using a DeltaVision platform (Applied Precision) composed of a customized inverted microscope (IX-71; Olympus), a UPlan Apochromat 100 × /1.4 NA oil objective, a camera (CoolSNAP HQ2 or 4.2Mpx PrimeBSI sCMOS camera; Photometrics), and a color combined unit illuminator (Insight SSI 7; Social Science Insights).

Figures were acquired using softWoRx v4.1.2 software (Applied Precision). Images were acquired every 5 minutes during 9 to 15 hours. To limit photobleaching, overnight videos were captured by optical axis integration (OAI) imaging of a 4.6-μm z section, which is essentially a real-time z-sweep.

Images presented in Figures 4, 6, S4, S5A, S6, and 2E were obtained using a spinning-disk microscope composed of an inverted microscope (DMI4000B; Leica) equipped with an HCX Plan Apochromat 100 × /1.46 NA oil objective and an UltraVIEW system

(PerkinElmer; including a real-time confocal scanning head [CSU22; Yokagawa Electric Corporation], solid-state laser lines, and an electron-multiplying charge coupled device camera [C9100; Hamamatsu Photonics]). Time-lapse images were acquired at 1 s interval using the Volocity software (PerkinElmer).

QUANTIFICATION AND STATISTICAL ANALYSIS

Fusion efficiencies were calculated as in [42]. Briefly, at the specified time post-starvation, mating pairs and fused pairs were quantified using the ImageJ Plugin ObjectJ, and the subsequent fusion efficiency was calculated using the following equation:

$$Fusion\ Efficiency = \frac{Fused\ Pairs}{Mating\ Pairs} \times 100$$

Fusion Times were calculated using the 5-minutes time lapse overnight movies using the 2-dots Myo52-tdTomato stage [42] as a marker for the beginning of the fusion process and either the entry of GFP expressed under control of the P-cell-specific p^{map3} promoter into the h- partner, or the maximum intensity of the Myo52-tdTomato dot, the two of which perfectly correlate [42], as a marker for the end of the process. Persistence times were calculated using the 5-minutes time lapse overnight movies using fusion time as beginning and last appearance of the Myo52-tdTomato dot as end of the post-fusion focus lifetime. Fusion times and persistence times vary between experiments because, for all experiments but Figures 1A and 1C, only early time points were considered to avoid Myo52 bleaching, which most certainly induces a bias toward quickly fusing cells. The WT control was imaged and quantified for each experiment to allow comparison within an experiment.

Fusion Focus intensities at fusion time were obtained using the 5-minutes time lapse overnight movies using either the entry of GFP into the h-partner, or the maximum intensity of the Myo52-tdTomato dot to determine the moment of fusion. On that time frame, a fluorescence profile across the fusion focus perpendicular to the long axis of the mating pair was recorded.

Profiles were background-subtracted and corrected for bleaching as follows: First, the cell fluorescence intensity was recorded over time in a square of 7x7 pixels in 12 control (non-mating) cell. These fluorescence profiles were averaged, and the mean was fitted to a double exponential:

$$Signal_{photobleaching-correction}(t) = Ae^{-Bt} + Ce^{-Dt}$$

We then used this fit to correct the fluorescence profiles across the fusion focus for photobleaching. After subtracting background signal, the value at each time point was divided by the photo-bleaching correction signal:

$$Signal_{BleachingCorrected} = \frac{Signal_t - Signal_{Background}}{Signal_{photobleaching-correction}(t)}$$

Corrected profiles were then either directly averaged and plotted, or further normalized to the mean of the WT maximum.

Patch to cytosol ratios were calculated from the ratio of the mean fluorescence intensity of 5 circular ROIs centered on patches (which gives the patch intensity) to the mean fluorescence signal of 5 circular ROIs centered on cytosolic signal per cell. The same operation was repeated on 36 cells and plotted.

Total fluorescence intensities in mating pairs were obtained using single snapshots on regular slides, 7h post-starvation, by outlining the mating pairs and recoding the mean fluorescence intensity for each of them. Background fluorescence was assessed by a small square ROI in an area devoid of cells on each image, averaged over all images, and subtracted from fluorescence intensity measurements.

The number of ectopic foci was assessed using the 5-minutes time lapse overnight movies during the fusion process between the 2-dot stage and the fusion time by simply counting the number of time-frames showing an ectopic Myo52-tdTomato or any other marker. The numbers vary between experiments because the DeltaVision camera was upgraded in the middle of the project, allowing us to detect more delocalization events. To assess colocalization at ectopic foci, single and double-color ectopic foci were identified as above and the colocalization was calculated with the following formula:

$$Percentage\ of\ Colocalization = \frac{2 \times EctopicFoci_{BothMarkers}}{EctopicFoci_{Marker1} + EctopicFoci_{Marker2}} \times 100$$

The proportion of ectopic foci containing a given marker was derived from the ratio of ectopic foci containing the given marker to the total number, which gave a ratio for each cell. That ratio was then averaged over all the recorded cells. For all experiments shown in Figure 6, only ectopic foci present at the cell sides were considered.

For3-3GFP retrograde flow was identified by visual inspection of spinning disk time-lapse imaging acquired at 1 s interval. Only linear For3 dot movements present over at least 5 consecutive time frames were considered. Dots were manually tracked using the ImageJ multi-point tool and instantaneous speeds calculated and averaged per track. Kymographs were constructed using the ImageJ reslice tool along a 5-pixel-wide line along the For3 dot track.

All plots, fittings, corrections and normalizations were made using MATLAB home-made scripts. For boxplots, the central line indicates the median, the circle, if present, indicates the mean, and the bottom and top edges of the box indicate the 25th and 75th percentiles, respectively. The whiskers extend to the most extreme data points not considered outliers. For bar plots, error bars represent the standard deviation. Statistical p values were obtained using a two-sided t test, after normal distribution had been

visually ckecked using a simple histogram. No further verification was made to ascertain that the data met assumptions of the statistical approach. All values below 0.05 are mentioned in the Figures, including sample size. Comparison with values above 0.05 are not shown (Figure 1A, *acp1Δ* and *acp1Δ acp2Δ* versus WT at 36h; Figure 2F, *fus1*^{G1087R,N1088P} *acp2Δ* versus *acp2+*; Figure 3F, Eng2-sfGFP in *acp2Δ* versus WT; Figure 6H). For all the supplementary figures, we consider, * < 5.10^{-2}, ** < 5.10^{-5}, *** < 5.10^{-8}. All experiments were replicated at least 3 times. There was no pre-selection of sample size, nor randomization or blinding. No data was excluded from analysis.

DATA AND CODE AVAILABILITY

This study did not generate any substantial code or dataset.

Current Biology, Volume *29*

Supplemental Information

Capping Protein Insulates Arp2/3-Assembled Actin Patches from Formins

Ingrid Billault-Chaumartin and Sophie G. Martin

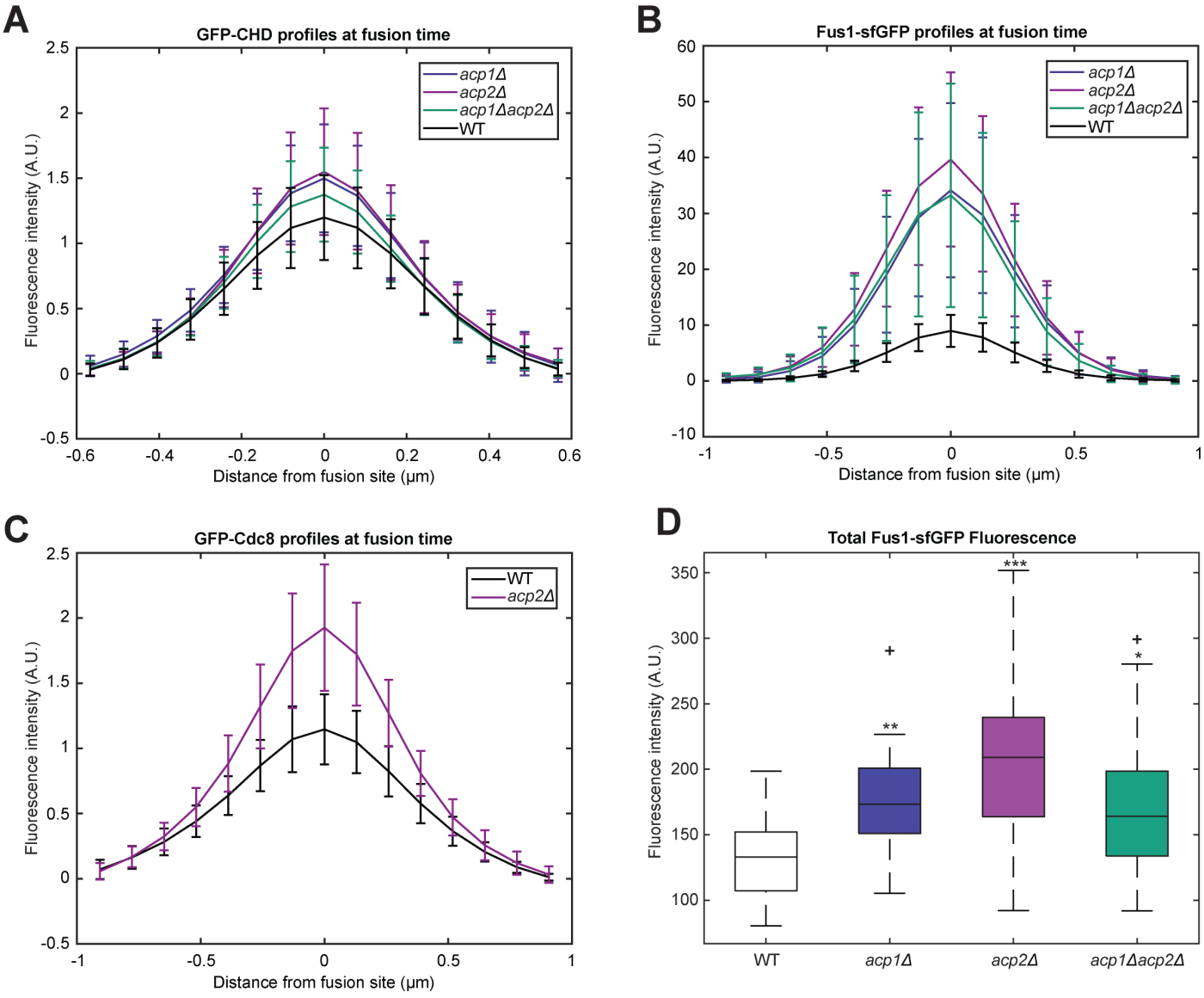

Figure S1. Quantification of the increase in actin, tropomyosin and Fus1 at the fusion focus in absence of CP. Related to Figure 2. A-C. Profiles of the bleach-corrected fluorescence intensities around the fusion focus at fusion time in the strains shown in Figure 2. The boxplot in Figure 2D shows the central points of these profiles further normalized to WT. (A) GFP-CHD profiles. p-values relative to WT are 5.4×10^{-4}, 2.9×10^{-4} and 2.5×10^{-2} (n = 40 mating pairs for each strain). (B) Fus1-sfGFP profiles. p-values relative to WT are 6.4×10^{-10}, 2.0×10^{-9} and 1.8×10^{-8} (n = 24 mating pairs for each strain). (C) GFP-Cdc8 profiles. p-values relative to WT is 1.3×10^{-8} (n = 24 mating pairs for each strain). **D.** Boxplot of total Fus1 fluorescence intensity in fusing cells, in WT and *acp2Δ*. p-value relative to WT are 3.0×10^{-6}, 1.6×10^{-8} and 8.7×10^{-4} This was measured on 32 mating pairs for each strain.

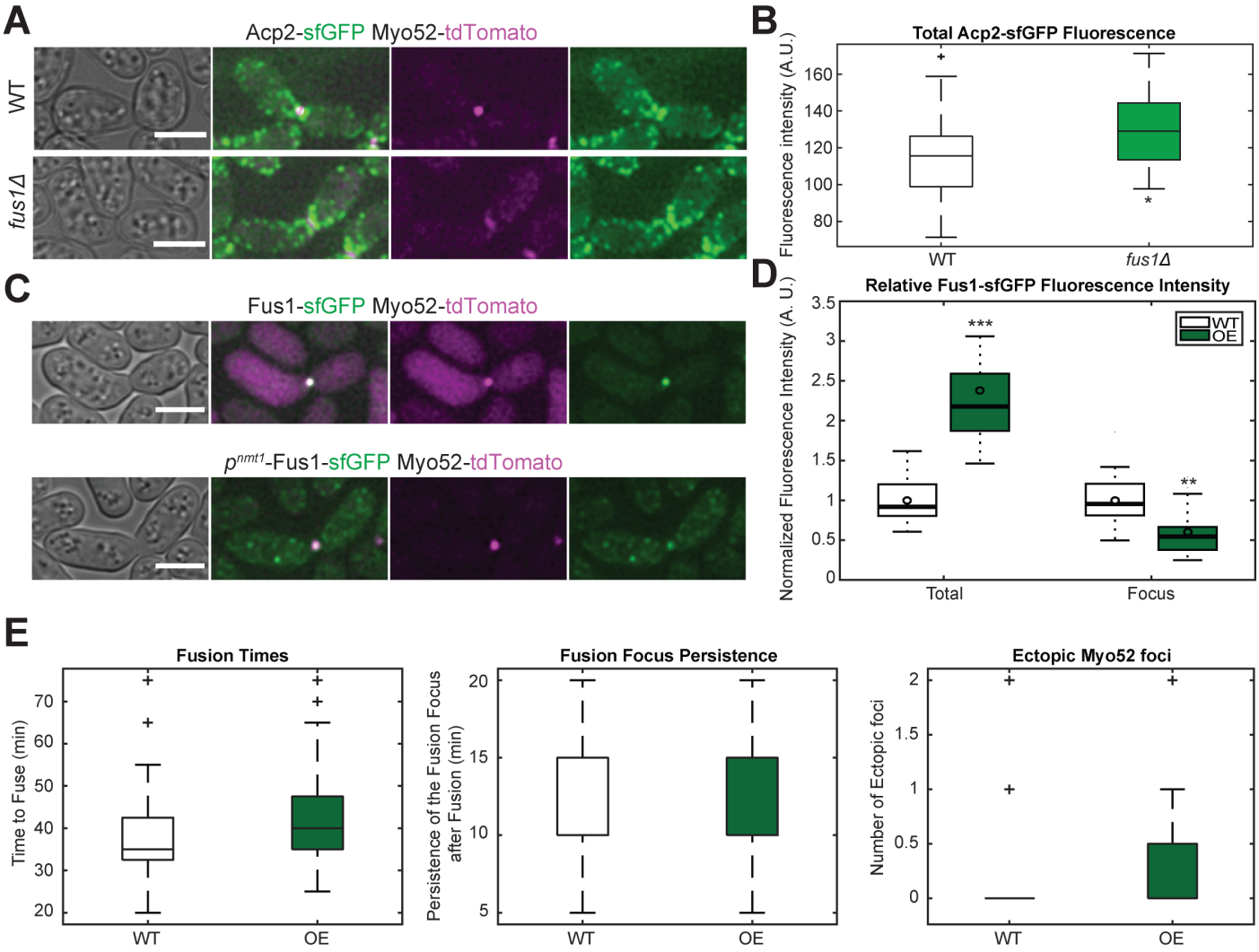

Figure S2. Weak increase in CP fluorescence in *fus1*Δ and no effect of Fus1 overexpression. **Related to Figure 2.** **A.** Myo52-tdTomato and Acp2-sfGFP in WT and *fus1*Δ at fusion time. **B.** Boxplot of total fluorescence intensities in fusing cells in strains as in (A). p-value relative to WT is 1.2×10^{-2} (n = 32 mating pairs for each strain). **C.** Myo52-tdTomato and Fus1-sfGFP at fusion time, in strains expressing Fus1 either from endogenous locus or, in addition, under the *nmt1* promoter. **D.** Boxplot of total and fusion focus fluorescence intensities normalized to WT in fusing cells in strains as in (C). p-value relative to WT is 1.3×10^{-12} for the total intensity (n = 15 and 45 mating pairs for WT and over-expressing cells) and 3.2×10^{-6} for the fusion focus intensity (n = 30 mating pairs each). Note that the quantified levels of overexpressed Fus1-sfGFP do not represent all Fus1 in the cell, as endogenous Fus1 is not tagged. **E.** Boxplots of fusion times, fusion focus persistence, and ectopic Myo52 foci in WT and Fus1-overexpressing strains. p-values relative to WT are 5.2×10^{-2} for fusion times (n = 60), 4.2×10^{-1} for persistence times (n = 60) and 3.7×10^{-1} for ectopic foci (n = 44 and 36 individual cells for WT and Fus1-overexpressing cells, respectively). Bars are 5µm.

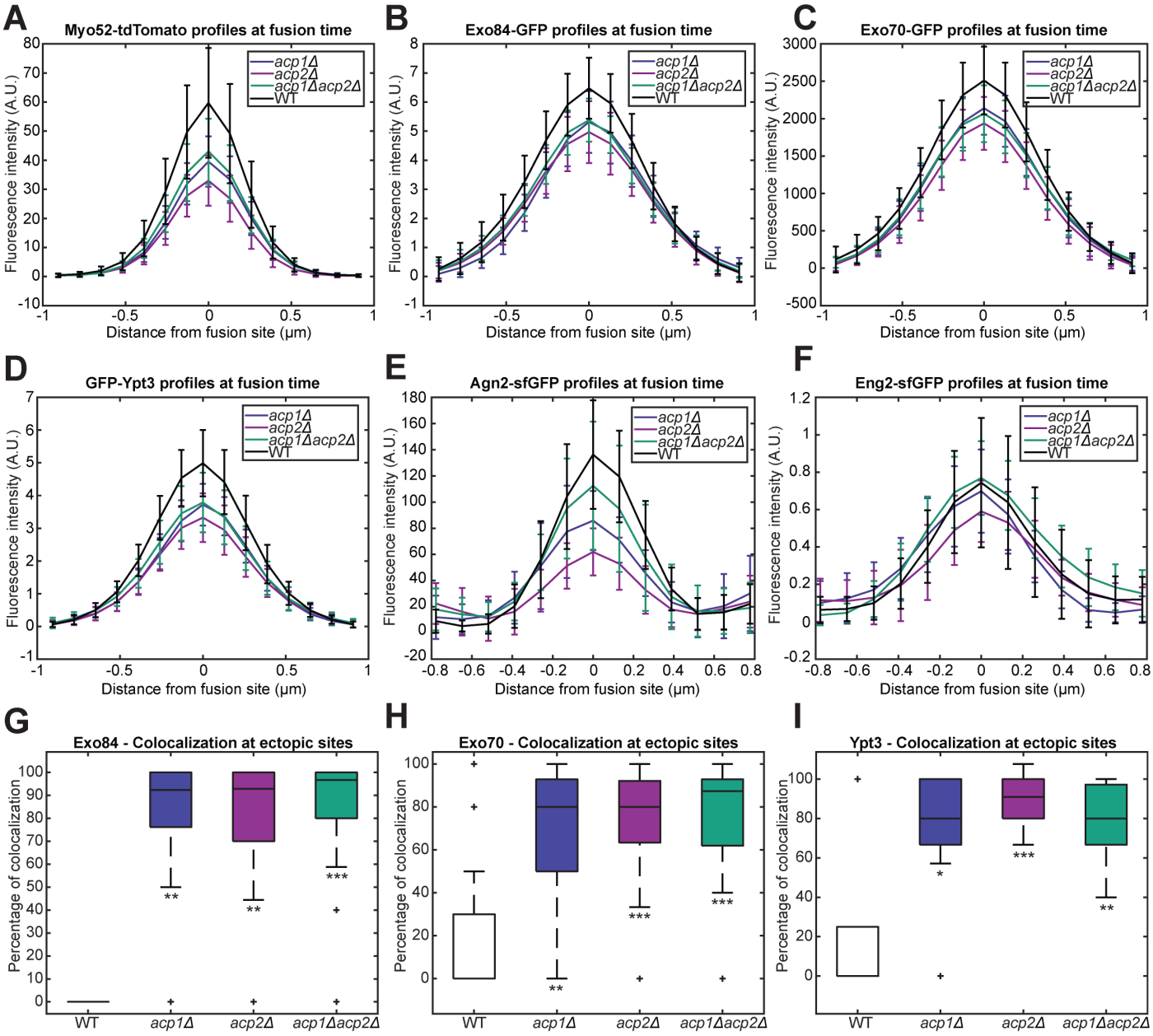

Figure S3. Quantifications of vesicular marker intensities at the fusion focus and ectopic foci in absence of CP. Related to Figure 3. A-F. Profiles of the bleach-corrected fluorescence intensities around the fusion focus at fusion time in the strains shown in Figure 3. The boxplot in Figure 3F shows the central points of these profiles further normalized to WT. (A) Myo52-tdTomato. p-values relative to WT are 3.2×10^{-8}, 3.7×10^{-11} and 1.4×10^{-5} (n = 40 for each strain). (B) Exo84-GFP. p-values relative to WT are 3.2×10^{-4}, 4.2×10^{-7} and 1.8×10^{-3} (n = 25 for each strain). (C) Exo70-GFP. p-values relative to WT are 1.1×10^{-4}, 3.4×10^{-8} and 3.0×10^{-6} (n = 40 for each strain). (D) GFP-Ypt3. p-values relative to WT are 3.1×10^{-7}, 1.2×10^{-9} and 1.1×10^{-5} (n = 30 for each strain). (E) Agn2-sfGFP. p-values relative to WT are 2.1×10^{-3}, 2.5×10^{-5} and 3.8×10^{-1} (n = 11 for each strain). (F) Eng2-sfGFP. p-values relative to WT are 7.2×10^{-1}, 1.0×10^{-1} and 8.4×10^{-1} (n = 11 for each strain). **G-I.** Boxplots of the colocalization of Myo52 with (G) Exo84, (H) Exo70, and (I) Ypt3 at ectopic sites in WT, *acp1Δ*, *acp2Δ*, and *acp1Δ acp2Δ* strains. p-values relative to WT are 1.1×10^{-7}, 8.7×10^{-7} and 6.0×10^{-9} for Exo84 (n= on 7, 16, 20, and 20 pairs respectively), 1.3×10^{-5}, 2.9×10^{-9} and 3.5×10^{-9} for Exo70 (n=28 for each strain) and 3.1×10^{-7}, 8.4×10^{-9} and 3.5×10^{-6} for Ypt3 (n=9, 29, 28, and 27 pairs respectively) for *acp1Δ*, *acp2Δ* and *acp1Δacp2Δ*, respectively.

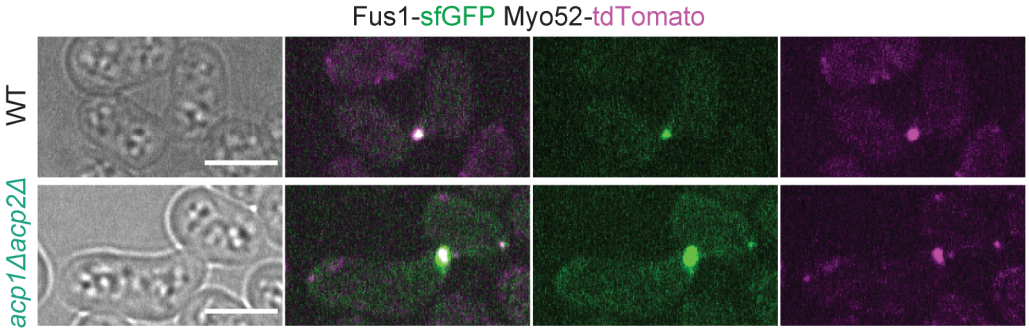

Figure S4. Fus1/Myo52 ectopic foci also form in capping protein double mutant strains. **Related to Figure 4.** Spinning-disk confocal microscopy images of Myo52-tdTomato and Fus1-sfGFP in WT and *acp1Δ acp2Δ* before fusion time. Bars are 5µm.

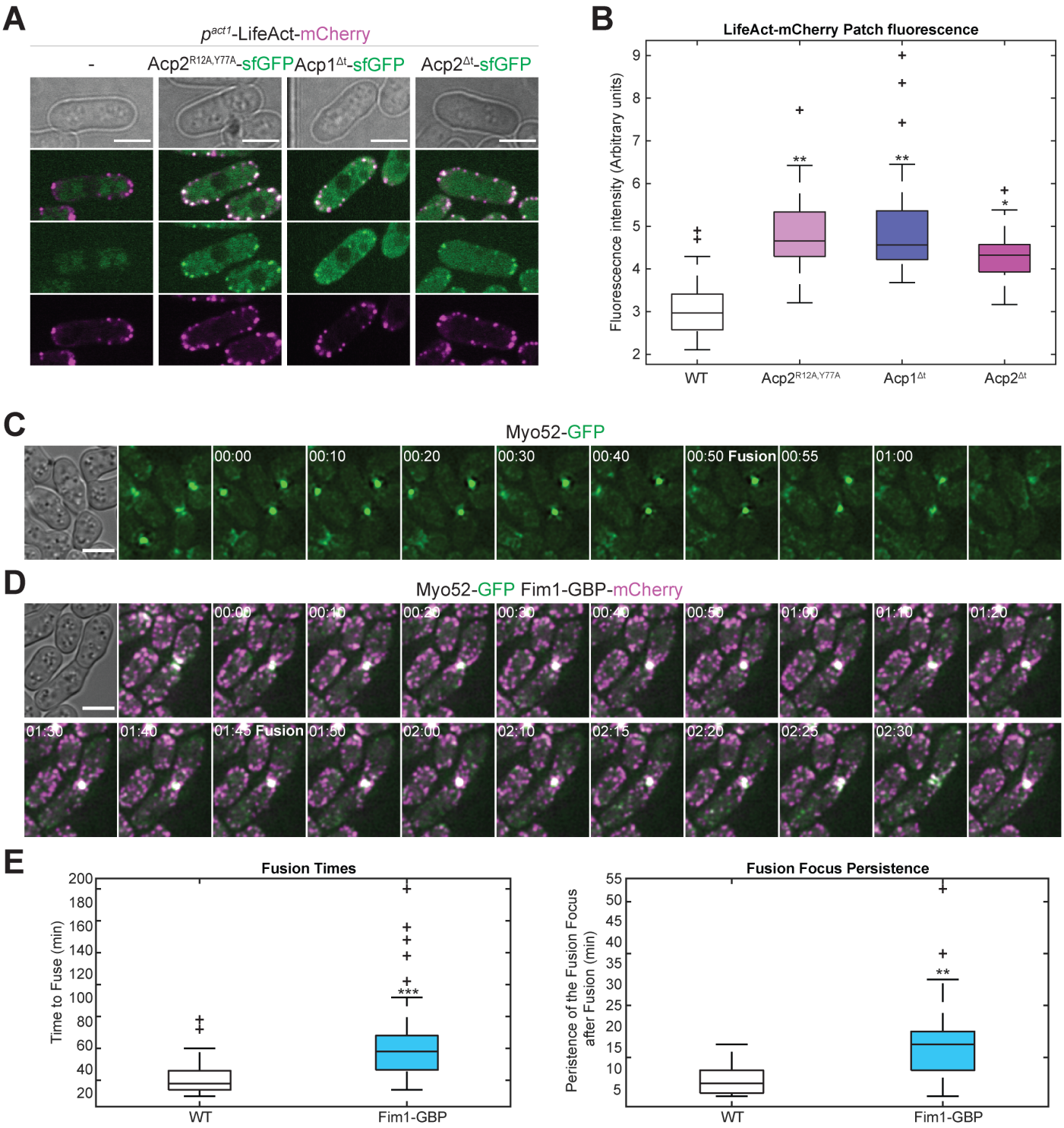

Figure S5. Actin levels are increased in *acp1* and *acp2* tentacle and CPI mutants and Forced recruitment of Myo52 to actin patches delays fusion. **Related to Figure 5. A.** Spinning-disk confocal microscopy images of LifeAct-mCherry under the actin promoter alone or in combination with Acp2^{R12A,Y77A}-sfGFP, Acp1$^{\Delta t}$-sfGFP and Acp2$^{\Delta t}$-sfGFP as described in Figure 5 in interphase cells during exponential growth. Bars are 5µm. **B.** Boxplots of LifeAct-mCherry patch fluorescence intensity in the strains shown in (A). p-values relative to WT are 1.3×10^{-7}, 1.6×10^{-6} and 1.4×10^{-4} (n = 30 cells for each strain). **C-D.** Time-lapse images of a strain expressing Myo52-GFP alone (C) or in combination with Fim1-GBP-mCherry (D) from beginning to disappearance of the fusion focus. The beginning is defined as the first formation of the focus in both cells. The fusion point is highlighted and is defined as the peak Myo52-GFP fluorescence intensity at the focus. Time in hour:min. Bars are 5µm. **E.** Boxplots of the above-mentioned strains fusion times and focus persistence times. p-values relative to WT are 2.1×10^{-8} and 9.5×10^{-8} for fusion times and persistence times, respectively (n = 55 mating pairs for each strain).

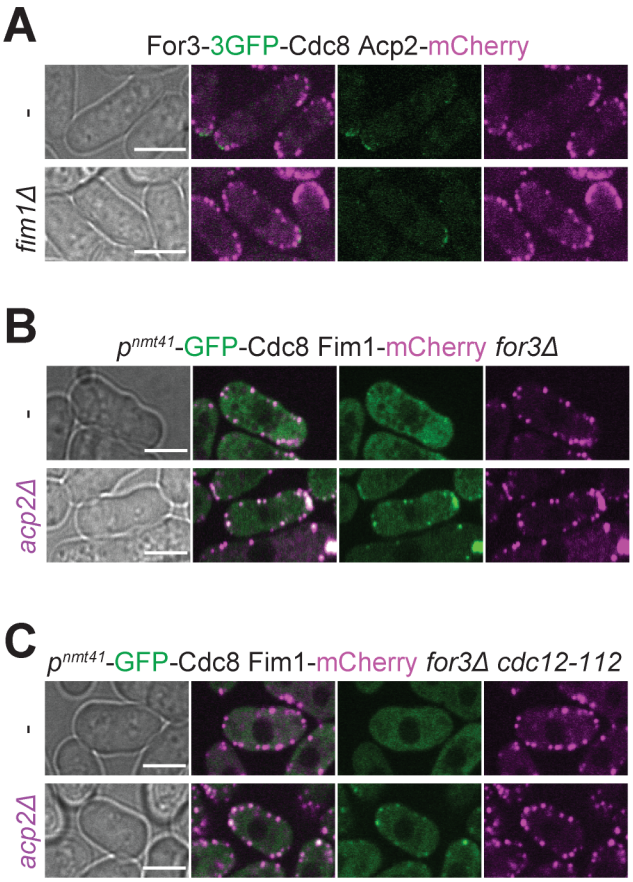

Figure S6. For3 does not localize to actin patches in *fim1Δ* cells and removing formins does not lead to the recovery of actin patch identity. Related to Figure 6. A. Spinning-disk confocal microscopy images of For3-3GFP and Acp2-mCherry in WT and *fim1Δ* cells. **B-C.** Spinning-disk confocal microscopy images of Fim1-mCherry and GFP-Cdc8 in interphase cells during exponential growth in (B) *for3Δ* and (C) *for3Δ cdc12-112* at 36°C, in otherwise WT and *acp2*Δ background. Bars are 5µm.

Oligonucleotides		
TTATCACTTGAAAATAATCATATATACGAAGAGCTTCGACTTTCAG AGTTGATAAACTTATTGGCTAAAGCTACATTACGGATCCCCGGGT TAATTAA *(Myo51 tagging)*	Sigma	osm3932
GAATATAGTATTAATGAGTACTAATATAAATTAAAAATATTGATCGG GTGTAACGTTTAATGATACTTGATAAAAAGCGAATTCGAGCTCGTT TAAAC *(Myo51 tagging)*	Sigma	osm4920
ATCTTTATTTTGCCAGAAGATATTGTGGCCGTTCGTCCTCGGTTG GTCCTTCATTTTATTGGCAGTTTAATGGCCGTACGGATCCCCGGG TTAATTAA *(Fim1 tagging)*	Sigma	osm2878
CGCAATATAAGTAATTAAATTGGGAAAAACACATGTGTTAAATCGT TTCGTTAAAAGCTATAGTTAAGTCGAAACAAAGAATTCGAGCTCGT TTAAAC *(Fim1 tagging)*	Sigma	osm2879
GAATTGCGTCGTCAACTTCCAGTCACTCGCCAGAAAATTAATTGG GAAAACGTTAGTGGCATCCGTATGAGAAATACTCGGATCCCCGG GTTAATTAA *(Acp1 tagging)*	Sigma	osm3416
AGGAAACAGCTTGAATCACCGTCTTAAAAAATATCGTCGCAAAAA AATTTCCAAAATTTATAAACACATATAAGTGTTGAATTCGAGCTCG TTTAAAC *(Acp1 tagging, full and tentacle deletion)*	Sigma	osm3417
TGCGGCATTGTCTTCACCATCCGTATTCGTTTCTTACCATTCACCA TTGTCCGCACCACATTATAGAAATTTCGAAAGCGGATCCCCGGGT TAATTAA *(Acp1 deletion)*	Sigma	osm4503
GCTCAAGTCGAAAATGGAATTCAACAGTCCTTCAACGTTGAACTT TCTTCACTTAATGACAAAAAGTTTAAAGAATTGCGGATCCCCGGG TTAATTAA *(Acp1 tentacle deletion)*	Sigma	osm5328
CATTAAGGCCTCACTTTTATTCTGAGATCGCTATCCGGTTGTATTC TTTTGTTTAAAGCATTATATCATCAACTCACCCGGATCCCCGGGTT AATTAA *(Acp2 deletion)*	Sigma	osm4504
CAATCTTTCTATGACTATTTTCGTTGAAGATGGAACGAATACTATG AGAAGATCACGGAAAGAAAACAAAAAGCAATCGAATTCGAGCTCG TTTAAAC *(Acp2 tagging, full and tentacle deletion)*	Sigma	osm4505
ACTCGTTCCATTCAACCCGTTTCCGATGCCCAACCAAATGATTCG GCTTTGCGTTCAGTTTTAAACGATCTTTCCATTCGGATCCCCGGG TTAATTAA *(Acp1 tagging)*	Sigma	osm4641
GAGGAAATGGAAACTCGGATGCGCAACTTCCTCCAGGATGTCTA CTTTGGAAAAACTAAAGATATCATCAACCAGACTCGGATCCCCGG GTTAATTAA *(Acp1 tentacle deletion)*	Sigma	osm5329
GCGGCCGCCATATGTTGTTCACTT *(Acp2 5'-ORF-sfGFP-kanMX-3' insert amplification)*	Sigma	osm5330
GCGGCCGCTTATTTCATGACCTT *(Acp2 5'-ORF-sfGFP-kanMX-3' insert amplification)*	Sigma	osm5331
GCATTAGATTTACTCGCACGATTAAACCC *(Acp2 R12A mutagenesis)*	Sigma	osm5432
GGGTTTAATCGTGCGAGTAAATCTAATGC *(Acp2 R12A mutagenesis)*	Sigma	osm5433
CCATGGAGCAATAAAGCTGATCCTCCTTTGG *(Acp2 Y77A mutagenesis)*	Sigma	osm5434
CCAAAGGAGGATCAGCTTTATTGCTCCATGG *(Acp2 Y77A mutagenesis)*	Sigma	osm5435
AAAGTCGACTGTTGCTTTGAATCATATTAC *(Fus1 5'-ORF-sfGFP-kanMX-3' insert amplification)*	Sigma	osm5449
CGTTTGATATCGATGTATTTACTGATTACTT *(Fus1 5'-ORF-sfGFP-kanMX-3' insert amplification)*	Sigma	osm5452
CTTCTAAACGGCTAGCTCAGCTTCATTGG *(Fus1 K879A mutagenesis)*	Sigma	osm5453
CAATGAAGCTGAGCTAGCCGTTTAGAAGG *(Fus1 K879A mutagenesis)*	Sigma	osm5454
CAAATGGTTAGTGCTCGTTTGCATAG *(Fus1 I951A mutagenesis)*	Sigma	osm5455
CTATGCAAACGAGCACTAACCATTTGC *(Fus1 I951A mutagenesis)*	Sigma	osm5456
GTCCTTCATATTCGTCCTTTTATGAATGATGC *(Fus1 GN1087,1088RP mutagenesis)*	Sigma	osm5457
CATCATTCATAAAAGGACGAATATGAAGGACC *(Fus1 GN1087,1088RP mutagenesis)*	Sigma	osm5458
GCTTCCATGATTGCTAATGACAAAACAG *(Fus1 K1112A mutagenesis)*	Sigma	osm5459
CCTGTTTTGTCATTAGCAATCATGGAAG *(Fus1 K1112A mutagenesis)*	Sigma	osm5460
TCCGGTACCGATCAGAAAATTATCGCC *(p^{nmt1} amplification)*	Sigma	osm3113
ACTGCGGCCGCTGATTTAACAAAGCGACTATAAGTC *(p^{nmt1} amplification)*	Sigma	osm3516
ACTGCGGCCGCATGATGACGGCTAGTTTTAAAGG *(fus1-sfGFP amplification)*	Sigma	osm3005
ACTGAGCTCTCTCTTAAGTTCATTGTTATTCTCC *(fus1-sfGFP amplification)*	Sigma	osm3006

Table S1. Oligonucleotides used in this work. Related to STAR Methods and Key Resources Table